

# Chapter 2

## Sum Frequency Generation Vibrational Spectroscopy of Silicone Surfaces & Interfaces

Dongchan Ahn and Ali Dhinojwala

### 2.1 Introduction

Silicone materials such as polydimethylsiloxane (PDMS) exhibit very unusual surface properties that arise from the unique flexibility, bond energy, partially ionic nature of the siloxane (Si-O) backbone, and low intermolecular forces [1, 2]. These molecular features are manifested in bulk properties such as low surface energy, heat stability, low temperature flexibility, dielectric strength, inertness, hydrophobicity, optical clarity and ease of crosslinking by a variety of mechanisms that have allowed silicones to grow from a research concept in the early 20th century to a virtually ubiquitous material set used in a remarkably diverse variety of industries and applications [3]. For example, Dow Corning Corporation, which was established in 1943, has grown to a \$6 billion company in 2010, based largely on silicones going into over 6,000 products spanning nearly every major commercial industry. In particular, the unique range of surface and interfacial properties attainable in a facile manner through the versatility of organosilicon chemistry positions silicones well for even greater future prominence as products and processes leverage structural control over ever-diminishing length scales.

Paramount to the effective development of micro- or nano-engineered materials are the structural and compositional insights from characterization of the interfaces. Despite remarkable advances in surface analysis techniques, elucidating direct structural information from interfaces remains difficult for a variety of reasons. Perhaps the most common challenge in surface science is the scarcity of the interface relative to large background signals from the ‘bulk’ that tend to result in poor sensitivity. Sum-frequency generation vibrational (SFG) spectroscopy offers

---

D. Ahn (✉)

Dow Corning Corporation, Midland, MI 48686, USA

e-mail: [d.ahn@dowcorning.com](mailto:d.ahn@dowcorning.com)

A. Dhinojwala (✉)

Department of Polymer Science, The University of Akron, Akron, OH 44325, USA

e-mail: [ali4@uakron.edu](mailto:ali4@uakron.edu)

intrinsic advantages in this regard, because the output is based on nonlinear optical selection rules that render it sensitive only to regions of a material where inversion symmetry is broken. In the majority of materials that are isotropic and homogeneous in the bulk, the technique is ideal for studying surfaces and buried interfaces non-invasively. The resulting output is an infrared (IR) vibrational spectrum that offers the same richness of molecular information and bonding with nearly unparalleled surface sensitivity.

While several general reviews of the applications of SFG appear in the literature, none have focused specifically on the application of SFG to silicones [4–10]. The reader is directed to these cited references for additional background and details on the technique and its use with other classes of materials. The unique and somewhat dichotomous surface properties of silicones, and their ever-increasing use in surface and interface-dependent applications such as lubricants, adhesives, micro-fluidic materials, sensors and matrices or scaffolds for nanocomposites, calls for increased fundamental understanding that has motivated the use of SFG analysis. The intent of this chapter is to focus specifically on the combination of this uniquely surface sensitive tool to study applications using PDMS and other silicone-based materials. We distinguish silicones from silicates and silanes by focusing on materials that have a flexible polymeric -Si-O-Si- backbone. For example, the body of references on SFG characterization of silane-based self-assembled monolayers or modified silica surfaces falls outside the scope of this review. We briefly overview the technique, then illustrate its utility in studying a number of important interfacial phenomena involving silicone-based materials by way of examples from the literature. Because the interpretation of SFG spectra can be quite complex, many of these examples highlight how SFG can be coupled with complementary techniques to provide a more complete understanding of interfacial effects. Lastly, we conclude by providing a summary of strengths, limitations and potential future opportunities for application of SFG and complementary techniques to silicone-based materials.

## 2.2 Fundamentals

### 2.2.1 Theory of Surface-Sensitive SFG

The theory of SFG has been explained in published works [11–14] and is not presented here at the same level of detail. The following background is sufficient for enabling the reader not familiar with SFG to understand the examples and case studies presented in the text [15].

When light interacts with a medium the polarization is expressed using the electric-dipole approximation as follows:

$$\mathbf{P} = \epsilon_0(\chi^{(1)}:\mathbf{E} + \chi^{(2)}:\mathbf{E}\mathbf{E} + \dots) \quad (2.1)$$

Here,  $\mathbf{P}$  is the polarization vector,  $\mathbf{E}$  is the electric field vector, and  $\chi^{(1)}$  and  $\chi^{(2)}$  are the first- and second-order electric susceptibility tensors of the medium (higher-order susceptibilities are not shown and are usually negligible in magnitude). Also,

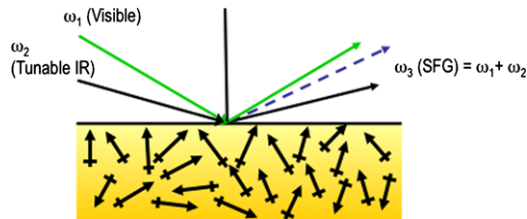


**Fig. 2.1** Schematic diagram (not to scale) of a copropagating, external-reflection (ER) geometry used for SFG. The beams of frequencies  $\omega_i$  are as follows:  $i = 1$ , S- or P-polarized visible; 2, S- or P-polarized IR; and 3, SFG. The SFG signal is detected after passing through a polarizer and filters

it is assumed that the medium does not have a permanent polarization (true for most organic materials). The second- and higher-order terms in the polarization equation are experimentally observed only when the medium is subjected to high electric field using a high intensity pulsed lasers. In infrared-visible SFG experiments, the medium is simultaneously subjected to two intense electric fields; then the induced polarization is as follows:

$$\mathbf{P} = \varepsilon_0(\chi^{(1)}:(\mathbf{E}_1 + \mathbf{E}_2) + \chi^{(2)}:(\mathbf{E}_1\mathbf{E}_2 + \mathbf{E}_2\mathbf{E}_1) + \dots) \quad (2.2)$$

The meaning of  $\mathbf{P}$ ,  $\mathbf{E}_i$ , and,  $\chi^{(j)}$  are the same as, or analogous to, those in (2.1).

When the source of electric fields is laser light as in Fig. 2.1,  $\mathbf{E}_1 = \mathbf{E}_1^0 \cos(\omega_1 t)$  and  $\mathbf{E}_2 = \mathbf{E}_2^0 \cos(\omega_2 t)$ ; therefore, it is easily seen with a trivial trigonometric rearrangement that the term containing  $\chi^{(2)}$  in (2.2) will have a sinusoidal component of frequency  $\omega_1 + \omega_2$  which shows that  $\chi^{(2)}$  is responsible for SFG. The  $\chi^{(1)}$  term is responsible for linear optical-processes such as Rayleigh and Raman scattering; however, unlike such scattering, the nonlinear SFG generates a coherent signal in the form of a collimated beam in a predictable direction. From symmetry arguments it can be shown that the third-rank tensor,  $\chi^{(2)}$ , has a value of 0 in centrosymmetric media if it can be assumed that only electric-dipole mechanisms are responsible for  $\chi^{(2)}$ , and the contributions from higher-order multipoles and magnetic dipoles are negligible (a usually good approximation). This is why SFG is forbidden in the bulk of most substances, but it is allowed at the interface between bulk phases where there can be no centrosymmetry.

Figure 2.1 shows a simple geometry for SFG that is commonly used. Here, the visible and IR beams are moving in the same direction along the  $x$  axis (copropagating), and all three beams are in the same plane, the plane of incidence. The  $\omega_1$  and  $\omega_2$  beams are either S- or P-polarized; S means the electric field of the light beam is perpendicular to the plane of incidence (along the  $y$  axis), and P means the field is in the plane of incidence (the  $xz$  plane). The signal-beam polarization is also set to S or P by the polarizer before the beam reaches the detector. The combination of polarizations of all three beams is given by a sequence of three letters, each being S or P (e.g., SSP), with the letters having the following meaning: polarization of the SFG beam, visible beam, and IR beam, respectively. The polarization settings

in SFG play an important role in selectively probing different components of  $\chi^{(2)}$  (discussed below).

If  $I(\omega_i)$  is the intensity of a beam at frequency  $\omega_i$  (see Fig. 2.1), then the SFG-signal intensity depends on the probing visible- and IR-beam intensities as follows [14]:

$$I(\omega_3 = \omega_1 + \omega_2) \propto |\chi_{\text{eff}}^{(2)}|^2 I(\omega_1) I(\omega_2) \quad (2.3)$$

Here,  $\chi_{\text{eff}}^{(2)}$  (or  $\chi_{\text{eff}}$  for simplicity) is an effective, second-order, nonlinear susceptibility of the interface; it is a sum of terms in which each term contains a single component of the second-order susceptibility tensor,  $\chi^{(2)}$ , of the interface; the components are  $\chi_{ijk}(\omega_2)$  (or  $\chi_{ijk}$  for simplicity), where  $i, j, k = x, y, z$  ( $x, y$ , and  $z$  are the lab axes in Fig. 2.1, and, from here on, the indices  $ijk$  appearing together will have this meaning). For an interface with azimuthal, or  $x$ - $y$ , isotropy (such as all the interfaces described below) only seven combinations of  $ijk$ , in  $\chi_{ijk}$ 's, out of the 27 possibilities are nonvanishing, and only four are independent:  $\chi_{xxz} = \chi_{yyz}$ ,  $\chi_{xzx} = \chi_{zyz}$ ,  $\chi_{zxx} = \chi_{zzy}$ , and  $\chi_{zzz}$ .

The combination of  $\chi_{ijk}$ 's that comprises  $\chi_{\text{eff}}$  depends on the beam polarizations: for example,  $\chi_{\text{eff}}$  in SSP polarization consists of just one term containing a single  $\chi_{ijk}$ .

$$\chi_{\text{eff, SSP}} \propto \chi_{yyz}(\omega_2) \quad (2.4)$$

The constant of proportionality in Eq. (2.4) has a weak dependence on  $\omega_2$ , and this dependence is often neglected. This equation shows that in SSP the  $\chi_{yyz}$  component of the  $\chi^{(2)}$  tensor is probed.

The  $\chi_{ijk}$ 's are each a sum of one nonresonant term and  $Q$  resonant terms, one for each vibrational mode of each interfacial species.

$$\chi_{ijk}(\omega_2) = \chi_{ijk}^{\text{NR}} e^{i\Phi} + \sum_{q=1}^Q \frac{\chi_{ijk,q}}{\omega_2 - \omega_q + i\Gamma_q} \quad (2.5)$$

where  $\chi_{ijk,q}$ ,  $\omega_q$ , and  $\Gamma_q$  are the line strength, frequency, and line width, respectively, of the resonance  $q$ , and  $\Phi$  is the relative phase of the nonresonant term with respect to the resonant terms. The SFG spectra are usually normalized for the variation in  $I(\omega_1)$  and  $I(\omega_2)$  Eq. (2.3). Often, spectra are then fit to Eq. (2.5), and the  $\chi_{ijk,q}$ 's obtained from the fit are then adjusted by any proportionality constant, such as in Eq. (2.4).

The  $\chi_{ijk,q}$ 's have their origins in the molecular hyperpolarizability-tensor ( $\beta$ ) components, which are as follows:<sup>1</sup>

$$\beta_{lmn}(\omega_2) = \sum_{q=1}^Q \frac{\beta_{lmn,q}}{\omega_2 - \omega_q + i\Gamma_q} \quad \text{where } l, m, n = a, b, c \quad (2.6)$$

<sup>1</sup>In Eq. (2.6), and the subsequent expressions that follow, we have assumed that all the vibrational modes,  $q$ , belong to a single type of molecular species or moiety. Although this is usually not true, the extension for the case of multiple types of species is trivial. The more general treatment would unnecessarily increase the complexity of the notation.

Here,  $a$ ,  $b$ , and  $c$  are axes of the Cartesian frame-of-reference that is fixed to the molecule;  $c$  is conventionally taken to coincide with the axis (or one of the axes) of highest symmetry of the molecule.  $\beta_{lmn,q} = A_{lm,q} M_{n,q}$ , where  $A_{lm,q}$  is the  $lm$  component of the Raman tensor and  $M_{n,q}$  is the  $n$  component of the transition-dipole-moment vector [16]. Therefore, only those vibration modes that are both Raman- and IR-active contribute to the hyperpolarizability tensor—i.e., only such modes are SFG-active.

The  $\beta_{lmn}(\omega_2)$  (or  $\beta_{lmn}$ 's for simplicity) can be projected on the lab axes ( $xyz$ ), given the orientation of the  $abc$  axes with respect to the  $xyz$  axes. This orientation is conveniently expressed using the Euler angles  $(\chi, \theta, \phi) = \Omega$  [11]. Knowing  $\Omega$ , the  $27 \times 27$  projection coefficients  $U_{ijk:lmn}(\Omega)$  can be determined and applied to obtain per-molecule components of  $\beta$  in the  $xyz$  frame as follows:

$$\beta_{lmn}(\omega_2, \Omega) = \sum_{l,m,n=a,b,c} U_{ijk:lmn}(\Omega) \beta_{lmn}(\omega_2) \quad (2.7)$$

The resonant portion of Eq. (2.5) is then a summation of the  $ijk$  component of hyperpolarizability for all interfacial molecules:

$$\begin{aligned} \sum_{q=1}^Q \frac{\chi_{ijk,q}}{\omega_2 - \omega_q + i\Gamma_q} &= \sum_{\text{molecules}} \beta_{ijk}(\omega_2, \Omega) \\ &= N \langle \beta_{ijk}(\omega_2, \Omega) \rangle \\ &= N \int \beta_{ijk}(\omega_2, \Omega) f(\Omega) d\Omega \end{aligned} \quad (2.8)$$

Here,  $N$  is the total number of such molecules,  $\langle \rangle$  indicates an ensemble average, and  $f(\Omega)$  is the probability distribution function of the molecular orientation.  $\theta$ , the tilt of the molecular  $c$ -axis from the surface normal ( $z$  axis), is of particular significance because often the molecules at the interface can be assumed to have azimuthal isotropy (randomly distributed in  $\chi$  and  $\phi$ ); in such cases,  $\Omega$  in Eq. (2.8) can be replaced by  $\theta$  (we shall assume this in what follows).

Substituting from Eqs. (2.7) and (2.6) in Eq. (2.8) gives

$$\chi_{ijk,q} = N \int \left[ \sum_{l,m,n=a,b,c} U_{ijk:lmn}(\theta) \beta_{lmn,q} \right] f(\theta) d\theta \quad (2.9)$$

$f(\theta)$  is usually assumed to be a Gaussian distribution, and clever methods to estimate the above integral have been devised [17]. Equation (2.9) shows the intimate connection between the components of the macroscopic susceptibility tensor,  $\chi^{(2)}$ , and its molecular counterpart, the microscopic hyperpolarizability tensor,  $\beta$ , of the molecular species that make up the interface. Herein lies the ability of SFG to determine the orientation of interfacial species; with a knowledge of  $\chi_{ijk,q}$  (obtained from SFG spectra),  $\beta_{lmn,q}$  (obtained from linear spectroscopies or computational methods), and a solution to Eq. (2.9), it is often possible to determine the tilt of molecular species,  $\theta$ , at the interface by taking ratios of appropriate  $\chi_{ijk,q}$ 's, and eliminating  $N$ ; in some cases, the ratio of  $\chi_{ijk,q}$ 's is independent of  $\beta_{lmn,q}$ 's, and it is possible to obtain  $\theta$  without knowing any  $\beta_{lmn,q}$ .

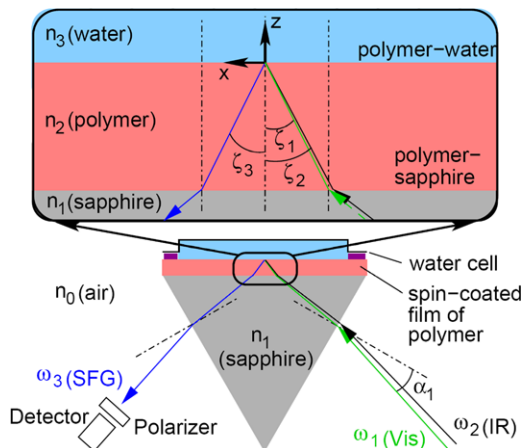


**Fig. 2.2** Schematic diagram (not to scale) of a TIR geometry used for SFG of a polymer–polymer interface. The beams of frequencies  $\omega_I$  have the same meaning as in Fig. 2.1. The mediums of refractive indices  $n_i$  are as labeled. The interfaces formed at the boundaries of these mediums are as follows: A and D, sapphire–air; B, polymer 1–sapphire; C, polymer 1–polymer 2. The incident angles ( $\omega_1$  and  $\omega_2$  beams) and the reflected/refracted angles ( $\omega_3$  beam) at these interfaces are denoted by  $\phi_{\text{interface}}$

Figure 2.2 shows another commonly used geometry for SFG measurements, called the total-internal-reflection (TIR) geometry; the figure shows an example of a polymer–polymer interface being probed by SFG. Here, one face of an equilateral, sapphire prism has two films of different polymers coated on it. The prism is then mounted on a cell (not shown) of an appropriate construction, and the incoming laser beams (at  $\omega_1$  and  $\omega_2$ ) are aligned as shown. The angle  $\alpha_1$  and  $\alpha_2$  are selected so that the incident and reflected angles at the polymer 1–polymer 2 (C) interface— $\zeta_{C,1}$ ,  $\zeta_{C,2}$ ,  $\zeta_{C,3}$ —are close to the critical angles for the visible, IR, and SFG frequencies at this interface. This set of  $\zeta_C$ 's greatly enhances the SFG signal from the C interface, while reducing any interfering signal from the polymer 1–sapphire (B) or polymer 2–air (D) interface [18, 19]. Therefore, proper choice of  $\alpha_A$ 's allows the selective probing of the C interface, but by choosing other values of  $\alpha_A$ 's, it is possible to selectively probe the B and the D interfaces, too. The setup shown here is for a polymer–polymer interface, but by replacing polymer 2 by a liquid (e.g. water) or gas (e.g. air), the polymer–liquid and polymer–gas interfaces can also be probed by appropriate selection of  $\alpha_A$ 's. Hence, we can appreciate the versatility of the TIR geometry.

### 2.2.2 Experimental Set-up and Sample Considerations

The study of silicone surfaces and interfaces requires either spin coating or dip coating a thin film on a solid substrate. The silicone films are cured by one of

the chemistries described below. In external-reflection geometry, the visible and infrared laser beams are incident on the films and the reflected SFG beam is collected (Fig. 2.1) and analyzed. In this external geometry, the SFG signal is generated at two interfaces, polymer-air and polymer-solid interfaces. The separation of the signal from these two interfaces is not trivial and requires solution of the linear and nonlinear Fresnel equations. By using different film thickness it is possible to find a range of film thickness where the SFG signals will be higher for either polymer-air or polymer-solid interfaces. This approach to separate the signals from both the interfaces has been demonstrated using polystyrene films [20]. In general, the signals from the polymer-solid interfaces are weak and are difficult to measure using external-reflection geometry [21]. However, the contributions from the solid interfaces cannot be known without any prior knowledge of the relative strength of the signals from both these interfaces. The use of plasma or UV to destroy or alter the SFG contribution from the polymer-air interface has been also used to confirm the relative contributions to the SFG spectra from both these interfaces [22].

The internal-reflection geometry described in Fig. 2.2 can be used to separate the contributions of the polymer-air and polymer-solid interfaces by changing the incident angle of the laser beams [23]. This geometry involves spin coating or dip coating polymer films on a sapphire prism. As a simple approximation, Snell's law can be used to determine the incident angles where the polymer-air and polymer-solid spectra can be collected. This technique was first demonstrated for polystyrene (PS) films and the orientation of the phenyl groups was shown to be very different for polystyrene in contact with air or sapphire substrate [23]. This approach was further extended to study polymer-polymer and polymer-liquid interfaces [15, 18, 24, 25]. The internal-reflection geometry was also used to study confinement of liquids between polymer in contact with sapphire or other polymer surfaces [26, 27]. The use of this geometry to study friction will be discussed later. The complete model for analyzing SFG spectra in internal-reflection geometry for polymer systems has been published recently [28]. This model highlights the conditions needed to use the internal-reflection geometry to obtain spectra for polymer-air (or liquid) or polymer-solid interfaces.

Both the internal and external geometry for SFG experiments are suitable for kinetic and temperature studies. The sample cells can be heated and the SFG spectra can be collected as a function of time and temperature. This technique has been used to study glass temperatures of thin films [29, 30], melting of molecules at interfaces [23, 31], kinetics of plasma treatment [32], and kinetics of rearrangements at polymer-liquid interfaces [10, 25, 33–35]. The collections of SFG spectra take from 5–20 minutes depending on the laser systems. This restricts the time scale for kinetic measurements. If the changes can be monitored without scanning the whole frequency range and instead can be monitored by changes in the peak intensity, changes on the time scale of seconds can be monitored as a function of time. With recent developments in femtosecond lasers coupled with CCD camera detection systems, the SFG spectra can be collected in milliseconds [36]. SFG is also very well suited to measure long time changes and in some recent work changes on the PDMS surfaces were monitored over a period of years [37].

### 2.2.3 Simulation

The intensity of the SFG signals can be related to the orientation of the molecules at the interface. Equation (2.9) describes the relationship between the macroscopic susceptibility and the orientation distribution of the molecules at the interface. Therefore, molecular models are often needed to interpret SFG spectra. A variety of known modeling approaches may be utilized depending on the complexity of the problem at hand. For well-defined systems such as self-assembled monolayers, the distribution can be assumed to be a Gaussian function with a very narrow width of tilt angles. One can model the polymer systems also using a Gaussian distribution and the average tilt angles and width of the distribution can be determined from the SFG spectra. However, the definition of the interface is often complicated for liquids and solids. The interface is not atomically flat and interfaces are not one molecular layer thick. Because of these complications, computational modeling and simulations are important complementary tools in understanding the SFG spectra. Naturally, it is important to select a tool that balances computational expense with a suitable level of structural detail at relevant length and time scales. In cases of phenomena such as wetting, interfacial tension, and chain orientation at complex interfaces, more extensive techniques such as molecular dynamics (MD) simulations are needed to ensure proper interpretation of SFG results.

The first comparison of MD and SFG results for polymers was done for PS films in contact with air [38]. The MD results provide information on the orientation and density of molecular units of polymer chains. The cosine average of tilt angle  $\langle \cos \theta \rangle$  is important in determining the intensity of the SFG signals. The maximum value is one when all the molecules are oriented at a tilt angle of zero with respect to the surface normal. The value of  $\langle \cos \theta \rangle$  is zero when the distribution of tilt angles is random or disordered. The MD simulations of PS showed that the orientation of phenyl groups is random in the center of the film and the symmetry is broken at the interface. The phenyl rings at the surface are facing outwards with tilt angle close to zero. The orientation of the methylene groups of the PS main chains are weaker than that of the phenyl groups and these results are in excellent agreement with the SFG results. The MD also revealed that the SFG signal does not originate from phenyl groups in the immediate vicinity of the surface. Instead the phenyl rings in the region as thick as 1 nm have non-zero  $\langle \cos \theta \rangle$  and they also contribute to the SFG signals. In addition, the SFG intensity is proportional to the product of the number density and  $\langle \cos \theta \rangle$ , and both these quantities are important in determining the strength of the SFG signals.

The MD results for PDMS films on glass substrate clearly showed that there is a break down in symmetry of the methyl groups in contact with air [39, 40]. Because of layering of molecules, using simple Gaussian models is incorrect. One needs to understand the average contributions of all these layers. For PDMS the analysis revealed that the methyl groups next to the solid surface are responsible for the strong SFG signals for PDMS in contact with sapphire coated with self-assembled monolayers. The consequences of these conclusions in the context of friction will be discussed later. The combination of MD and SFG is extremely important in understanding the orientation and density of molecules at complex surfaces or interfaces.



## 2.2.4 Silicone Cure Systems

Many of the best known applications of silicones, such as sealants, adhesives, coatings and rubbers, involve PDMS in its cross-linked, or ‘cured’, elastomeric form. The versatility and convenience of organosilicon chemistry is evident in the variety of cross-linking mechanisms (or cure systems) that can be used to convert PDMS and other silicone polymers into solids with the aforementioned unique surface and bulk properties. A more detailed discussion is deferred to references on organosilicon chemistry and silicone rubber technology [1, 41, 42], but we briefly describe two of the most common general curing schemes for PDMS because both the static and dynamic surface properties of silicone elastomers can be influenced by the cure system. Additionally, this serves to denote key functional groups that can be observed by SFG to monitor the effects of surfaces and interfaces on curing reaction kinetics and stoichiometric balance.

First, consider an addition cured PDMS such as the widely studied Sylgard® 184 elastomer. The cross-linking occurs through a hydrosilylation reaction between the elastically active vinyl (Vi) terminated PDMS chain ends with a multifunctional silicon hydride (SiH) cross-linker to form an end-linked network with no leaving groups or by-products. In addition, additives such as fillers, adhesion promoters and cure modifiers may introduce Vi or SiH functional groups to ensure their incorporation into the network.

Hydrosilylation requires a catalyst, typically a Pt or Rh complex, and is accelerated by heat, making it well suited for rapid continuous assembly or coating applications. Hence, this is a very widely used system for curing silicone rubbers and coatings. In this chapter, silicone elastomers can be assumed to be cross-linked by this chemistry unless otherwise noted. The cure rate can be modified by a variety of additives to achieve a desired working time, or pot life, after the various components are combined. However, inadvertent cure inhibition can occur by the presence of certain additives, substrates, or even atmospheres that contain other catalyst-coordinating compounds such as those containing S, P, Sn, or N. Because cross-linkers, catalysts and additives are typically small molecules or oligomers, they are prone to interface segregation resulting in composition gradients near surfaces and interfaces [43, 44]. The consequence of segregation is to alter the effective stoichiometric balance in these regions and the resulting properties. The ability of SFG to detect the infrared spectrum from interfaces makes it a useful tool to track the fate of reactive groups involved in curing or adhesion. Common IR fingerprint regions for functional groups of interest in hydrosilylation curing silicone matrices include SiH ( $2100\text{--}2200\text{ cm}^{-1}$ ) and Si-Vi ( $1600\text{ cm}^{-1}$ ), which can be compared against the characteristic C-H stretching from Si-methyl groups on a PDMS backbone ( $2960\text{ cm}^{-1}$  asymmetric and  $2910\text{ cm}^{-1}$  symmetric) [45].

Another common class of cure systems is based upon hydrolysis and condensation of hydrolysable silicone polymers. Variants generally involve combinations of linear polymers capped by either  $\text{-OH}$  or alkoxy-silyl terminal groups that react with cross-linkers that are typically organosilanes multifunctional in alkoxy-silane or

other hydrolysable groups capable of undergoing condensation. While many variants exist, the most common condensation cure systems are catalyzed by organotitanium or organotin compounds and are often controlled by the in-diffusion of moisture and out-diffusion of alcohol or acidic leaving groups. In reality, the organometallic compounds are not classic catalysts because they may participate as reactants and are incorporated into the network [46]. These cure systems are commonly utilized to cross-link silicone sealants and caulks used in household and construction applications. In some cases, such as acetoxycured sealants that give off the familiar vinegar scent while curing, the reaction is driven forward by the formation and subsequent evaporation of acidic leaving groups on exposure to moisture, requiring relatively low organometallic catalyst loadings. Because cross-linking is typically performed at ambient conditions and is generally slower than heated addition cure systems, concentration gradients can be even larger in condensation cured materials [47–49]. Additionally, both the leaving groups and the unreacted residual groups can have very significant implications on adhesion because of their polarity. Useful IR fingerprints regions for functional groups of interest in condensation curing silicone matrices include Si-O-CH<sub>3</sub> (2830–2850 cm<sup>-1</sup>), SiOH (broad 3700–3800 cm<sup>-1</sup> and 3200–3450 cm<sup>-1</sup>), and for acetoxycured silicones, -C=O (1750 cm<sup>-1</sup>) [45].

## 2.3 Applications of SFG to Silicone Surfaces and Interfaces

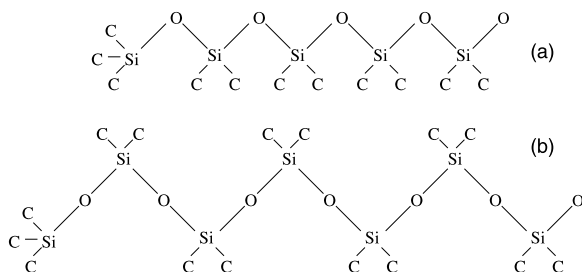
### 2.3.1 *Silicone Surface Orientation and Rearrangement*

A number of unique surface properties of siloxanes are often attributed to the unusual backbone flexibility and mobility of their polymer chains. PDMS surfaces are often reported to be quite dynamic, and terms such as rearrangement, restructuring, reorganization or hydrophobic recovery are used to describe these changes with limited insights to the mechanisms and underlying chain conformations. Highlighted below are examples where SFG has been used to probe these effects at the molecular level.

#### 2.3.1.1 *Silicone/Air and Silicone/Water Interfaces*

The siloxane backbone is very flexible, and the glass temperature of high molecular weight PDMS is typically observed near 150 K. The flexibility of PDMS chains can result in two potential conformations and could either expose methyl groups at the surface or more polar oxygen atoms. The low surface energy of PDMS surface could favor either of these two conformations because the methyl groups could face the air interface. However, PDMS also shows unusually high water contact angles that are very stable with time. Because the chains are very flexible and mobile they could potentially restructure to expose the more polar oxygen groups at the PDMS-water

**Fig. 2.3** A schematic showing the two possible orientations of PDMS chains. Hydrogen atoms are not shown for clarity. Reprinted from Ref. [39] with kind permission of © The American Institute of Physics (2003)



interface, as shown in Fig. 2.3(a). However, the stable high water contact angles suggest that the structure in Fig. 2.3(b) is more preferred. The Si-O-Si bonds are not planar as suggested in this two-dimensional picture and the structure (b) provides the least steric constraints in packing of the bulky methyl groups. The molecular dynamics simulation results show that the methyl groups cover the surface of PDMS in contact with air [39]. In contact with water, the simulation results show sharpening of the orientation of the methyl groups [50]. While subtle changes in orientation, such as ‘flattening’ of the average methyl group bond angle away from water surface have been reported experimentally [51], no large scale cooperative reorganization events such as the complete inversion of structure as shown in Fig. 2.3(a) were observed in the simulations. This explains the stable water contact angles even though the chains are flexible and have the mobility to restructure and adopt different conformations. Other observations of dynamic contact angle changes of PDMS/water are attributed to chemical changes from process by-products [52] or side reactions involving small numbers of reactive groups such as cross-linker molecules [53]. The simulation results also showed a small amount of hydrogen bonding between water and silicon atoms. These simulation results are consistent with the SFG results that show methyl groups at the PDMS-air [40], PDMS-water [51], and also PDMS in contact with polymer surfaces [54, 55]. We note that the presence of methyl groups of PDMS at the water interface has important consequences in adhesion of cells, bacteria, and biocompatibility [56, 57].

### 2.3.1.2 High Energy Surface Treatment Effects

Various forms of high energy treatment of PDMS are often used to render PDMS surfaces more hydrophilic for applications in microfluidics, bioengineering and lithography. The most common of these surface treatment methods are based upon exposure to various types of plasma, long wavelength ultraviolet (UV) or short wavelength UV-ozone (UVO) sources (see also Chap. 3). All three methods have been studied by a variety of conventional surface analytical techniques that indicate that under appropriate exposure conditions, the exposed silicone surface is oxidized to various extents into a silsesquioxane or silicate layer through a complex set of potential free radical- and anion- promoted oxidation mechanisms [2, 58–62]. However, optimization of these techniques is largely empirical because of limited understanding of the physico-chemical processes at the surface and near-surface regions. Additionally, these treated surfaces are often reported to be time dependent,

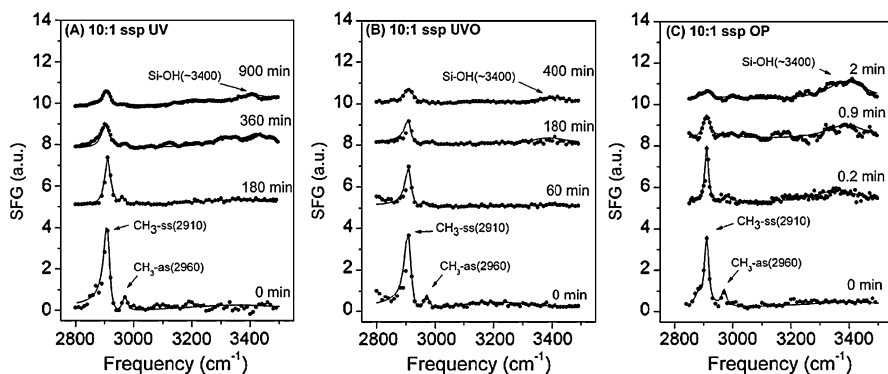


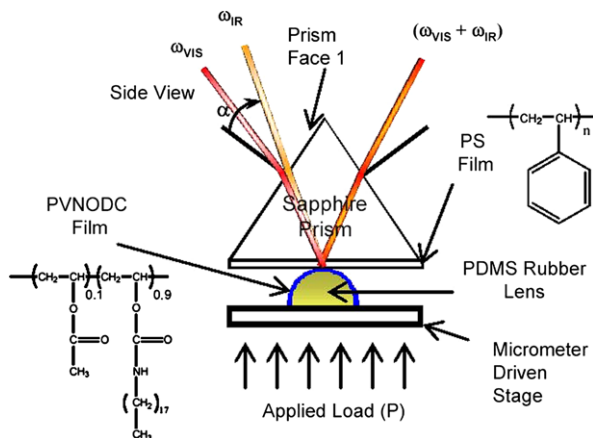
**Fig. 2.4** SFG spectra showing surface chemical changes of Sylgard® 184 silicone elastomer induced by various exposure times to (A) UV, (B) UV-ozone and (C) oxygen plasma treatments. Reprinted from Ref. [58] with kind permission of © The American Chemical Society (1996)

with contact angles that can rapidly increase with aging time in air after the treatment, a phenomenon called hydrophobic recovery. Many studies indicate that this recovery originates from migration of low surface energy siloxane oligomers that are created by chain scission of PDMS [2]. This effect can obscure the interpretation of data from post-mortem techniques that cannot be conducted in situ or under ambient conditions. Hence, the surface sensitivity and relatively rapid acquisition in ambient conditions make SFG an excellent complement to develop the better mechanistic understanding needed to optimize these methods. Ye et al. used SFG to study the effects of treatment time by oxygen plasma (OP), UV and UVO treatments on Sylgard® 184 prepared at two different crosslinking stoichiometries (10:1 vs. 4:1 base to curing agent mix ratios) [58]. In the case of UV and UVO, the SFG spectra were obtained in situ. All three techniques resulted in a decrease in  $-\text{CH}_3$  and  $-\text{CH}_2-$  groups, and the formation of  $\text{Si}-\text{OH}$  groups, which is consistent with increased hydrophilicity caused by silicate formation (Fig. 2.4). The loss of surface  $-\text{CH}_3$  groups was reported to follow first order kinetics, with OP providing the fastest response, followed by UVO and UV. The OP also resulted in virtually complete removal of  $-\text{CH}_3$  within 2 min, unlike UVO and UV. The persistence of residual  $-\text{CH}_3$  at the surface is consistent with a higher proportion of radical-based chain scission events in the UV techniques. Such experiments illustrate the power of SFG to provide mechanistic insights needed for more precise surface modification by high energy techniques

### 2.3.2 Friction and Lubrication

Mechanical contact between two soft solids, particularly polymers, is of fundamental importance in the areas of friction, adhesion, and contact mechanics. Although there have been numerous studies on measurements of adhesion and friction using

**Fig. 2.5** Schematic of the experimental geometry used to probe the mechanically formed contact interface between two polymer surfaces using TIR-SFG. One polymer film is coated on the sapphire surface and the other on top of a deformable elastomeric lens. In this case, the lens is coated with poly(vinyl *n*-octadecyl carbamate-co-vinyl acetate) (PVNODC). Reprinted from Ref. [63] with kind permission of © Taylor & Francis Group (2005)



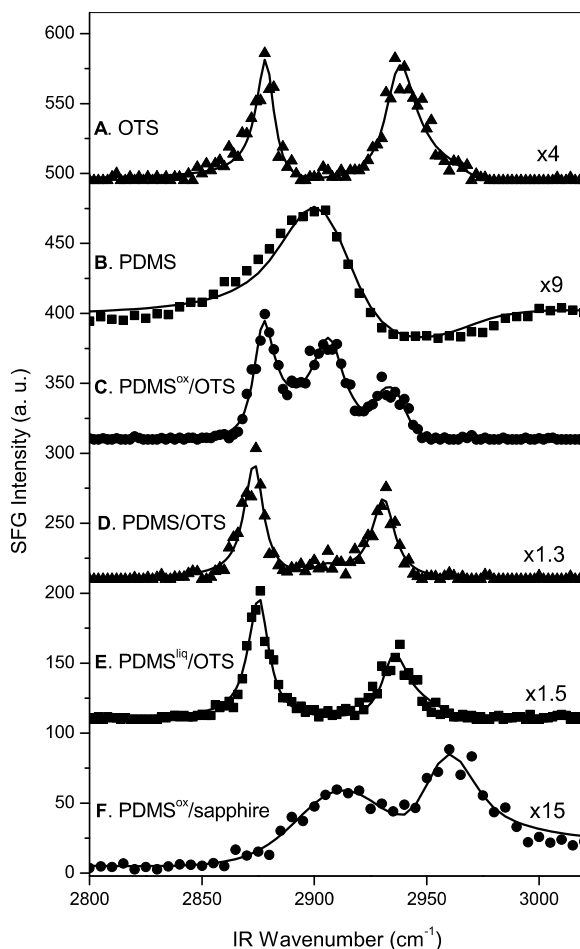
macroscopic and microscopic contact areas, there have been no direct measurements of interfacial structure during mechanical contact between two polymer surfaces. In order to understand adhesion hysteresis, friction, and mechanisms of energy dissipation at interfaces, it is important to study the structure of polymer surfaces upon mechanical contact.

### 2.3.2.1 Probing Contact Interfaces

SFG in internal-reflection geometry was used to directly probe the contact interface between an elastomeric lens and a solid surface [63]. The soft elastomeric semispherical PDMS lens provides a uniform and smooth contact area for studying friction and adhesion in conjunction with SFG (Fig. 2.5). The size of the contact area can be easily controlled by varying the normal force and the radius of curvature of the PDMS lens. Moreover, by depositing films of different polymers on the elastomeric lens, this geometry can be used to study the interface between many different polymers and can be easily adapted to incorporate in situ friction and adhesion force measurements. The usefulness of this geometry was first demonstrated by studying the mechanical contact of a comb polymer with PS films [63]. The structure of the interface upon mechanical contact was very different from the interface after annealing.

The ability of SFG to study the contact or buried interfaces was used to study PDMS in contact with solid surfaces [40]. Figure 2.6 shows SFG spectra in SSP polarization for various PDMS surfaces in contact with sapphire or sapphire surfaces coated with hydrophobic self-assembled monolayers. Figures 2.6A and 2.6B are SFG spectra for octadecyltrichlorosilane (OTS) and crosslinked-PDMS surfaces before contact. No differences in the SFG spectra were observed for crosslinked and oligomeric PDMS surfaces. Figure 2.6A is a typical spectrum for a well-packed OTS monolayer with ordered methyl groups. The methylene peaks are absent for an all-trans conformation. In Fig. 2.6B, the two main peaks are assigned to the

**Fig. 2.6** SFG spectra of (A), OTS; (B), PDMS; (C), PDMSox/OTS; (D), PDMS/OTS; (E), PDMS<sup>liq</sup>/OTS; and (F), PDMSox/sapphire. The solid lines are fits to the square of the sum of the Lorentzian functions Eq. (2.1). (B) and (F) are taken with a broader wavenumber resolution (full width half maximum (fwhm)  $\sim 20 \text{ cm}^{-1}$ ) to improve the signal-to-noise ratio. The SFG spectra were offset along y-axis by an arbitrary amount and were scaled for clarity. In (C) and (D) for OTS, the methyl Fermi band is slightly red shifted and the ratio of the symmetric methyl and methyl Fermi intensity has changed upon contact. This effect is reversible as the spectra before and after contact are indistinguishable. Reprinted from Ref. [40] with kind permission of © The American Chemical Society (2005)



methyl groups bonded to silicon (symmetric vibration at  $2906 \text{ cm}^{-1}$  and asymmetric vibration at  $2962 \text{ cm}^{-1}$ ). In the case of PDMS surface treated with short oxygen plasma treatment (PDMSox), the oxygen plasma treatment oxidizes the surface and the SFG spectrum from  $2800\text{--}3200 \text{ cm}^{-1}$  does not have any resolvable features. Figure 2.6C shows the spectrum for PDMSox-OTS interface. The silicone methyl peak is extremely strong at this interface. Since the PDMSox surface before contact has no methyl peaks, this indicates a significant interfacial reconstruction. The presence of PDMS chains after interfacial reconstruction is also evident in the adhesion experiments that show reduced hysteresis. For the PDMSox/OTS contact, once the highest load is reached the reconstruction is completed and the unloading proceeds with an equilibrium interface. The strain energy release rate on unloading is equal to  $43 \text{ mJ/m}^2$ . This value is similar to that expected for the thermodynamic work of adhesion, which between PDMS and OTS is around  $40\text{--}45 \text{ mJ/m}^2$ . These adhesion measurements of PDMS/OTS and PDMSox/OTS are consistent with the SFG

results. A strong adhesion and adhesion hysteresis is observed for PDMS/sapphire contact due to the formation of hydrogen bonds between the hydroxyl and silicon groups. The adhesion hysteresis decreases significantly at the PDMS<sub>ox</sub>/sapphire interface due to the enrichment of the interface in low molecular weight PDMS chains, thus forming a weak boundary layer (less energy dissipation due to reduced chain pull-out). Consequently, based on the adhesion results, the PDMS<sub>ox</sub>/sapphire interface has reconstructed with the diffusion of short PDMS chains.

### 2.3.2.2 Long term Aging Effects

PDMS is widely used as a model elastomer to study adhesion and friction. Because of the robustness of the platinum catalyst used for crosslinking, hydrophobicity, transparency, and nanometer-smooth surfaces, it is used in the areas of soft lithography, release coatings, biomaterial, and medical implants. However, it was shown recently by Kurian et al. [37] that the surface of PDMS is not stable with time. The friction and adhesion of PDMS lenses in contact with a glassy methacrylate polymers, showed an unusually high adhesion hysteresis and friction for PDMS lenses that were stored for an extended period of time (aged lenses) as compared to those that were prepared and used within a week (fresh lenses). This effect was very reproducible, and these results could not be explained by contamination of the lenses during storage or by the generation and segregation of short oligomeric PDMS chains upon aging. Additionally, the authors did not observe any differences between the aged and fresh samples using x-ray photoelectron spectroscopy (XPS) and contact angle measurements.

To understand the effect of aging, Kurian et al. [37] studied the contact interface between PDMS lenses and poly(*n*-propyl methacrylate) (PPMA)-coated sapphire prisms using the SFG spectroscopy in the TIR geometry. They observed no differences between the aged and unaged lenses at the PDMS/PPMA interface in static contact, even though there were striking differences in adhesion and friction properties. Interestingly, the biggest differences were observed only after sliding PDMS lenses on the PPMA-coated surface. The SFG intensity of the PDMS Si-CH<sub>3</sub> symmetric peak increases by almost three orders of magnitude upon sliding the aged lens on the PPMA (Fig. 2.7). This dramatic increase in SFG signal could only be due to alignment of PDMS chains at the contact interface. These measurements were conducted on aged lenses after extracting them in toluene to remove the short oligomeric chains and this ruled out the possibilities of short oligomeric chains affecting the SFG results. The nearly identical nature of the surface of aged and unaged lenses suggests that the differences due to aging are very subtle and indistinguishable in a static contact. The authors postulated that aging results in chain scission that disrupts the cross-linking and increases the density of the surface anchored chains with one free end. These surface anchored chains are stretched during sliding as postulated by the earlier theories in the area of rubber friction by Schallamach [64]. The authors also postulated that the stretching of chains also leads to

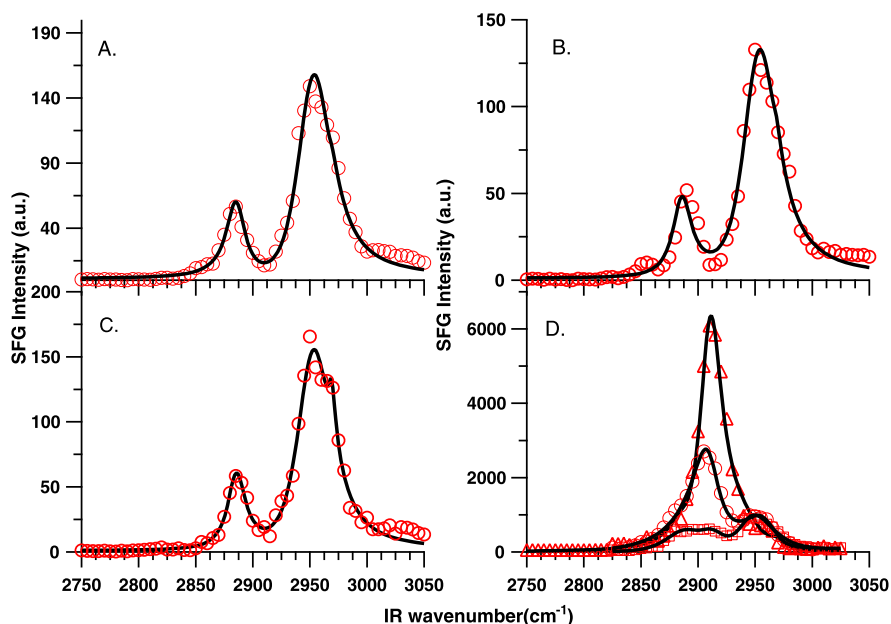


**Fig. 2.7** SFG spectra in SSP polarization of a fresh PDMS lens/PPMA interface in contact (A) and after sliding (B). The spectrum remains unchanged for fresh lens after friction experiment. SFG spectra of aged lens/PPMA interface in contact (C, 18 month aged lens) and after sliding (D, aging time: 4 months (*box*), 8 months (O), and 18 months (*triangle*)). The data for 4 and 8 months in (D) are scaled by 7 times for clarity. The solid lines are the fits to the data using a Lorentzian equation. Significant enhancement in  $2910\text{ cm}^{-1}$  peak, as a function of aging time, is observed upon sliding of aged PDMS lens. Reprinted from Ref. [37] with kind permission of ©The American Chemical Society (2010)

ordering of these molecules at the interface. Interestingly, the ordering is not permanent and the surface structure relaxes after stopping the sliding. These relaxation time constants are much higher than those expected based on bulk viscosity.

### 2.3.2.3 Probing Acid-Base Interactions

The molecular interactions at interfaces govern the wetting, adhesion, friction, chemical reactions, and many other material and biological phenomena at interfaces. Techniques such as heat of mixing in dilute solutions are employed to determine the strength of the donor–acceptor interactions. Kurian et al. [65] have used SFG to directly determine the strength of the donor–acceptor interactions by probing the shift in the vibrational peaks at buried interfaces. The authors have demonstrated the application of this spectroscopic technique to determine the interaction energies of various polar and nonpolar polymers in contact with the sapphire substrate. Because SFG does not require dilute solutions or the use of common solvents, it is widely applicable for determining interaction energies for many other solid–solid interfaces



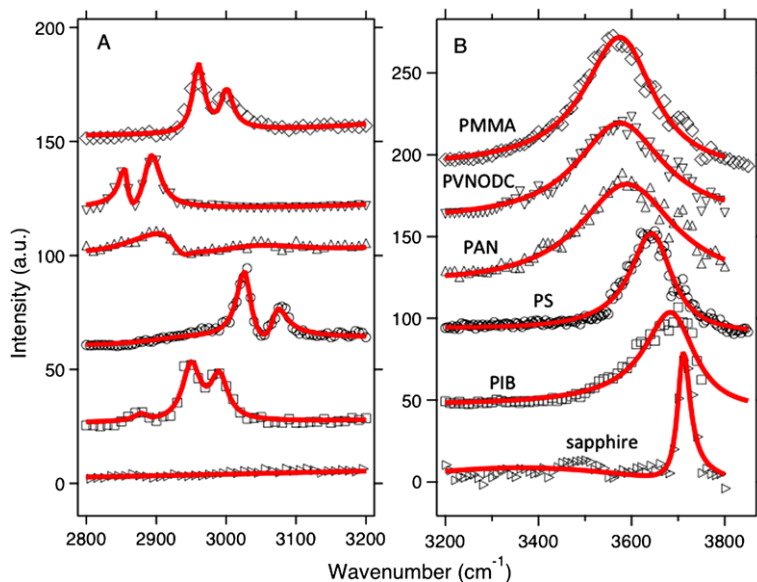


**Fig. 2.8** (A) SFG spectra of hydrocarbon region for interface of sapphire with air (*right triangle*), PIB (*box*), PS (*circles*), PAN (*triangle-up*), PVNODC (*triangle-down*), and PMMA (*diamond*). (B) Hydroxyl region interfacial SFG spectra for the interfaces reported in (A). All the spectra were collected at room temperature using P-polarized input and SFG beams. The *solid lines* in (A) and (B) are the fits using the Lorentzian equation. Reprinted from Ref. [65] with kind permission of © The American Chemical Society (2010)

that are important in the areas of adhesion, tribology and wetting. The application of this direct spectroscopic technique to determine the interaction energies of various polar and nonpolar polymers in contact with the sapphire substrate was demonstrated. The SFG spectra in PPP polarization for these polymers in contact with the sapphire substrate are shown in Fig. 2.8. The interaction energies determined from the shift do not correlate with water-contact angles which clearly demonstrates the importance of molecular rearrangement in contact with the sapphire substrate. For example, the octadecyl side chain polymer poly(vinyl *n*-octadecyl carbamate-co-vinyl acetate) (PVNODC) exhibits a very high water contact angle (110°, similar to polyisobutylene (PIB)). However, the interaction energies of PVNODC with the sapphire substrate are closer to the ester interaction of poly(methyl methacrylate) (PMMA). These differences are due to the molecular rearrangement of the octadecyl side chains in contact with the sapphire substrate which increases the interactions of the polar groups (carbonyl or N-H) with the surface OH. This rearrangement is also observed in the differences in the orientation of the methyl and methylene groups. Another interesting example is that of poly(acrylonitrile) (PAN) in contact with sapphire. Even though PAN has the lowest water contact angle (60°) among the five polymers studied, the interaction energies are not as high as PMMA (water contact angle of 73°). This is due to the strong affinity between the CN-CN groups (within the polymer) compared to the CN-surface OH interactions. Lachat et al.

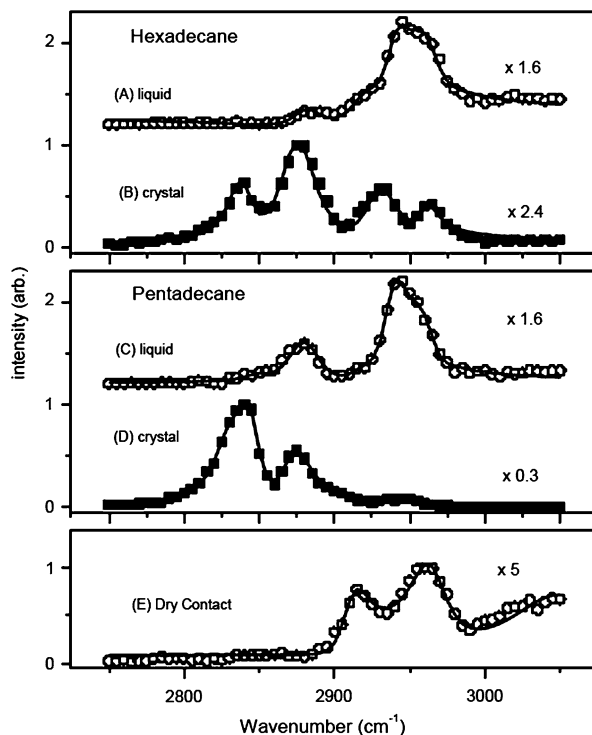
have also observed a shift in the CN peak due to the interactions of the CN group with the surface OH groups [34]. PIB is the most hydrophobic polymer Kurian et al. [65] have studied and the small red shift of  $30\text{ cm}^{-1}$  is similar to that of sapphire in contact with nonpolar pentadecane. PS is in between the more polar PMMA and PIB due to the interaction of the phenyl groups with the sapphire substrate. While silicone systems were not studied in this work, the technique to determine subtle non-covalent molecular interactions such as acid-base interactions has obvious relevance for better understanding of interfacial contributions to silicone lubrication, release and adhesion.

#### 2.3.2.4 SFG Studies of Lubricated Sliding

Liquids confined between two solid surfaces are important in understanding friction and wear of lubricated surfaces. Tires on roads, windshield wipers, movements of human joints are some examples where flexible-rigid contact interfaces are experienced. There has been a long standing discussion on whether the structure of liquids confined between two surfaces is different from that in the bulk. Experiments by Robert and Tabor using rubber lenses in contact with glass substrates concluded that the bulk viscosity of confined liquids were similar to those in the bulk for thicknesses as small as 25 nm [66]. Due to surface roughness, Tabor's experiments were inconclusive for a thickness less than 25 nm. Using atomically smooth mica surfaces, Israelachvili and coworkers have studied nanometer thin films and have shown that oscillatory force profiles are observed for a variety of liquids due to layering of molecules under confinement [67]. These results are supported by results from computer simulations. As a consequence of layering, the Newtonian liquids show solid-like response under confinement. Nanjundiah et al. studied confinement effects of small linear alkanes trapped between PDMS and sapphire substrate using SFG [26]. This novel approach of using flexible elastomeric lenses that deform against flat solid surfaces to confine molecules offsets the need to have perfectly parallel surfaces.

Nanjundiah et al. [26] measured the SFG spectra of confined hexadecane and pentadecane above and below the bulk melting points (Fig. 2.9). The SFG spectra upon confinement are different from unconfined hexadecane and pentadecane in contact with sapphire substrate. The confinement-induced ordering can be inferred from the higher SFG signals (3 times higher than liquid spectra), and the presence of methyl symmetric mode and weak methylene symmetric mode. Both the confined and bulk pentadecane liquid spectra have strong methyl asymmetric signals, which indicates methyl groups are on average tilted with respect to the surface normal. Pentadecane confined crystal/sapphire interface is dominated by the presence of a strong methylene symmetric peak at  $2840\text{ cm}^{-1}$  along with the methyl symmetric and methyl Fermi resonance modes. The SFG intensity for confined pentadecane crystal is higher than that of confined pentadecane/sapphire interface. The presence of strong methylene symmetric mode is surprising and suggests that the structure of the confined crystal structure is very different from bulk pentadecane

**Fig. 2.9** SFG (SSP) spectra of hexadecane (A) and pentadecane (C) confined liquid/sapphire interfaces at 295 K. The SSP spectra for confined hexadecane (B) and pentadecane (D) crystal/sapphire interfaces were taken at 287 and 279 K, respectively. The dry PDMS/sapphire SFG spectrum is shown in (E). Reprinted from Ref. [26] with kind permission of © The American Physical Society (2005)



crystal/sapphire interface. The strong methylene intensity in confined crystal cannot be accounted for by the presence of gauche defects as in the case of liquid alkane/sapphire interfaces. Nanjundiah et al. [26], with the help of a simple model, postulated that the confined pentadecane chains are crystallizing with the chains lying flat next to the sapphire substrate. These results have important implications in our understanding of friction and lubrication in confined geometry.

Nanjundiah et al. [27] showed that the confinement of water between PDMS and sapphire substrate was very different from that of alkanes. The sliding of the PDMS lens in the presence of water shows lower friction than dry sliding. The frictional forces for wet sliding were much higher than those expected for lubricated sliding. The authors proposed that the water is not expelled from the contact spot with regions where the PDMS is in direct contact with the sapphire substrate which can explain the higher friction coefficient than that expected from lubricated contact. Roberts and Tabor have also observed higher friction for a rubber sliding on a glass surface in the presence of water [66]. They concluded that the higher friction was due to asperity contact rather than higher viscosity of confined water, as depicted in Fig. 2.10. The SFG results agree with the hypothesis of the PDMS sliding on wet sapphire surface with asperity contacts. The asperity contacts are where the PDMS methyl groups are coming in direct contact with the surface hydroxyls on the sapphire substrate.

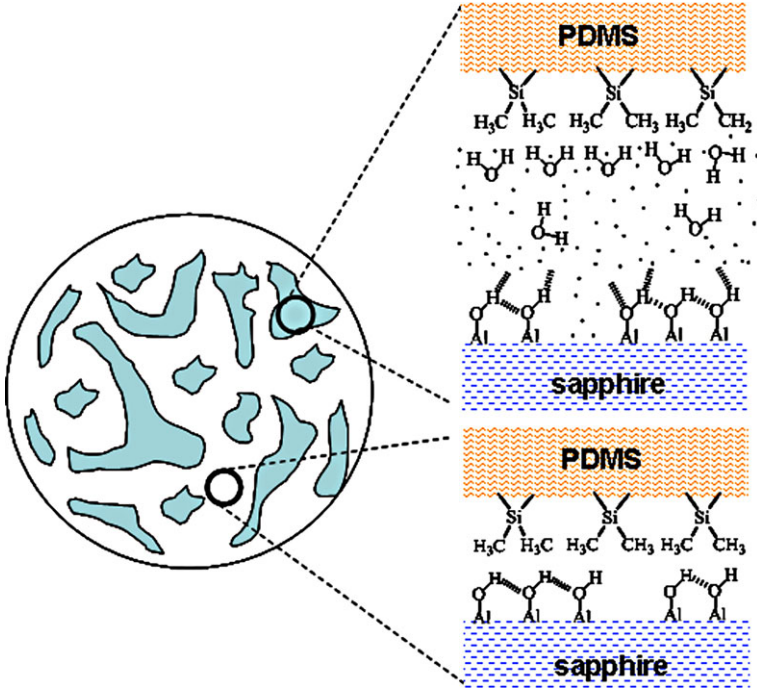


**Fig. 2.10** A sketch of the contact region formed between the PDMS lens and the sapphire surface in the presence of confined water. A tentative physical picture of the molecular structure in these two types of contact region are also shown on the right. The relative size of those two regions cannot be quantified from these results and the area and size selected in the sketch are only for visual aid. Reprinted from Ref. [27] with kind permission of © The American Institute of Physics (2009)

### 2.3.3 Adhesion

Pressure-sensitive adhesives (PSAs) and release coatings differ considerably from curable adhesives and sealants in their mechanism of adhesion. Therefore, we present these topics separately. A key difference is that PSA materials rely upon non-covalent interactions across the interface that are coupled multiplicatively by bulk energy dissipation mechanisms to give the measured adhesion or release profile. Mathematically, this can be expressed concisely for any type of elastomeric adhesive by the following empirical relationship based upon the form proposed first by Gent and Schulz [68, 69]:

$$\mathcal{G} = W[1 + \Phi(a_T v)] \quad (2.10)$$

Here,  $\mathcal{G}$  is the energy release rate, the practical adhesion energy measured by some adhesion or release test,  $W$  is the thermodynamic work of adhesion, and  $\Phi$  is a bulk viscoelastic loss function which is dependent on the crack growth velocity ( $v$ ), which is in turn governed by the rate of testing, reduced by the Williams–Landel–

Ferry (WLF) shift factor for time-temperature superposition ( $a_T$ ) [70].<sup>2</sup> For our purposes this empirical relation captures the essential physics of practical adhesion, the key feature being the multiplicative interplay of  $W$  and  $\Phi$ . It is important to emphasize that  $\Phi$  is usually the dominant term with most elastomers, often causing  $\mathcal{G}$  to be many orders of magnitude larger than  $W$ . However, this can only be so when  $W$  is sufficiently high that the mechanisms of bulk dissipation can be invoked to raise the product to an appreciable value, a fact that is borne out mathematically in the limit where  $W$  approaches zero. In other words, no matter how optimally “lossy” the bulk properties of the adhesive are, this cannot overcome an inherently weak interface; adhesion always starts with the interface. As shown by the aforementioned recent studies of acid-base interactions [65], SFG allows one to study both non-covalent and covalent interfacial interactions responsible for  $W$ .

### 2.3.3.1 Pressure-sensitive Adhesion and Non-covalently Bonded Interfaces

To this point commercial silicone pressure-sensitive adhesives and release coatings have not been studied by SFG. However, Roan has used SFG to gain insights on the interfacial segregation of certain functional groups in hydrocarbon-resin tackified acrylic PSA's [71]. Further, as discussed in the preceding section, SFG has been coupled with the interfacially sensitive Johnson, Kendall and Roberts (JKR) adhesion test method (see also Chap. 1) to probe the origins of adhesion hysteresis in contact interfaces between surface-modified PDMS elastomers and solid substrates, which is fundamentally relevant to mechanisms of adhesion and release [40]. It is noteworthy that the hydrosilylation cure chemistry used for cross-linking the lenses is the relevant system for both silicone PSAs and release coatings, the majority of which are addition cured. Therefore, significant opportunities remain to enhance current state of understanding of silicone release coatings and PSAs that is based largely on bulk measurements [72–74] by using SFG to study interface structure and composition.

### 2.3.3.2 Curable Adhesives and Reactive Interfaces

Curable silicone adhesives differ considerably from PSAs in that they are dispensed in place as an uncured, flowable composition that undergoes one or more reactions to crosslink into a gelled solid with adhesion to the substrate. Examples of curable silicone adhesives range from moisture-cured construction sealants and caulks to heat-cured adhesives for microelectronics or medical devices. These applications typically require durable, irreversible adhesion to the substrate that preferably develops simultaneously during the curing process through chemical coupling reactions with the substrate surface. While primers or surface pre-treatments may be used, it is generally more desirable to use a self-priming, or primerless, adhesive to eliminate

---

<sup>2</sup>Although Eq. (2.10) is valid only at thermodynamic equilibrium, it can be generalized to accommodate non-equilibrium conditions by substituting for  $W$  some inherent value of adhesion  $G_0$  usually regarded as rate-independent.

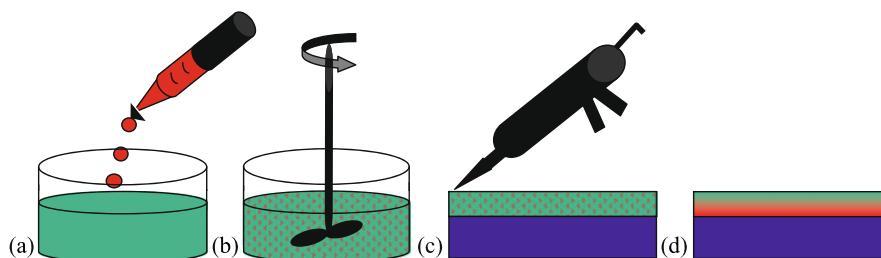


**Fig. 2.11** Idealized representation of key steps in the preparation of a self-priming adhesive: (a) addition of adhesion promoter (*red*) to a curable silicone elastomer formulation (*green*), (b) mixing of the formulation, (c) dispensing of the adhesive onto a substrate (*blue*), and (d) curing of the adhesive in which the adhesion promoter migrates to the substrate interface

the additional time and cost associated with pre-treatment. In essence, the ideal adhesive is one in which a low concentration of adhesion promoters is homogeneously blended into the uncured silicone composition but selectively migrates to the substrate interface during the curing process to effectively form a primer layer in situ, as depicted in Fig. 2.11.

In some cases, the coupling chemistry may involve the same groups as crosslinking, but often the reactions must be completely different to accommodate different types of substrate. Because of the drastic change in physical properties that occur and the complex array of competing reaction-diffusion events that ultimately determine the interface structure and composition, the mechanisms of adhesion are difficult to ascertain. In cases where strong adhesion develops, the interface by definition cannot be separated readily for study by conventional surface analytical techniques. Hence, the molecular sensitivity and ability of SFG to study buried interfaces non-destructively has motivated several SFG studies of curable silicone adhesives.

#### 2.3.3.2.1 Silane Orientation at Amorphous Polymer Interfaces

Perhaps the most common class of adhesion promoters, or coupling agents, for self-adherent curable adhesives is the alkoxysilanes [75]. These react under mild conditions with a variety of substrates and do not generally interfere with Pt cure catalysts. Despite their wide use, there remain many unanswered questions regarding their mechanisms of adhesion, particularly to plastics and other non-metallic substrates lacking an obvious reactive site. Chen et al. took the first step in understanding such effects by studying the orientation of neat silane coupling agents in contact with various plastics [76]. Both the nature of the tri-functional silane ‘head-group’ (trimethoxysilyl vs. trichlorosilyl) and the organo-functional tail (octadecyl vs. aminopropyl), and their resulting interactions with the polymer substrates, were found to profoundly influence the interfacial orientation of the coupling agents on PS or PMMA substrates. To eliminate background signals from the substrates, they used deuterated PS (d-PS) and PMMA (d-PMMA) to study the silane orientation, and saw large spectral differences (Fig. 2.12a) that could be interpreted qualitatively by the schematics in Fig. 2.12b.

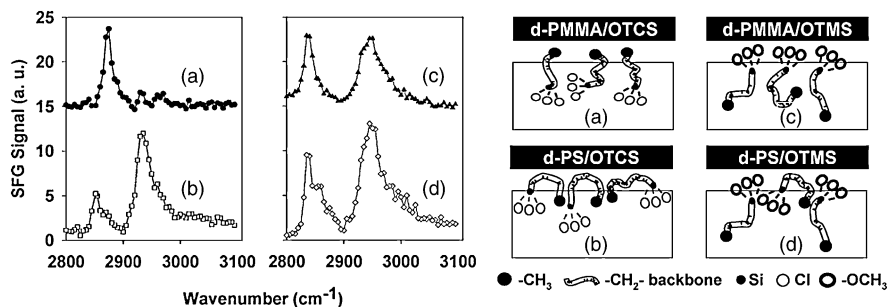


**Fig. 2.12** (Left) Summaries of SFG spectra (SSP) collected from various polymer/silane interfaces: (a) d-PMMA/octadecyltrichlorosilane, (b) d-PS/ octadecyltrichlorosilane, (c) d-PMMA/octadecyltrimethoxysilane, (d) d-PS/octadecyltrimethoxysilane. (Right) Corresponding schematic representations of silane orientation deduced from these spectra. Reprinted from Ref. [76] with kind permission of ©The American Chemical Society (2003)

Chen et al. [76] also studied the response of the non-deuterated PMMA side of the interface. By monitoring the  $2955\text{ cm}^{-1}$  peak signal characteristic of the symmetric stretch of the ester methyl group of PMMA, they found that exposure to the aminopropyltrimethoxysilane (ATMS) caused a time-dependent loss of signal that indicated a complete loss of interfacial order after about 100 s of contact. In contrast, the PMMA interfaces with octadecyl trichlorosilane (OCTS) and octadecyltrimethoxysilane (OTMS) retained a stable, finite signal after initial exposure.

### 2.3.3.2.2 Aminosilane Diffusion into Polymer Films

Further studies of the dynamics of aminosilane/PMMA interfaces by Chen et al. confirmed that the transient loss of SFG signal was due to diffusion of the silane into the polymer substrate [77]. By testing against d-PMMA films of different thicknesses, they were able to use SFG to monitor the structure of the silane diffusion front and estimate a diffusion coefficient of approximately  $4 \times 10^{-13}\text{ cm}^2\text{ s}^{-1}$ , several orders of magnitude smaller than most other small molecules (Fig. 2.13). Further, they observed rapid diffusion of the aminosilane into PS thin films in a bilayer experiment. This experiment demonstrates the power of SFG to simultaneously study both the structure and dynamics of very slow diffusional processes that would be very difficult and time consuming to study by conventional means such as attenuated total reflectance infrared (ATR-IR) spectroscopy. Such a technique could be further exploited to understand the interplay between the diffusional processes that control interfacial self-assembly of coupling agents and any concurrent bulk and interfacial reactions, and may yield new mechanistic insights on penetrant/polymer interactions.

### 2.3.3.2.3 Silane Adhesion Promoters for Pt-Cured Silicone Elastomers

Because of their effectiveness as penetrants into glassy polymer surfaces and fast reactivity with moisture, aminosilanes can serve as effective adhesion promoters



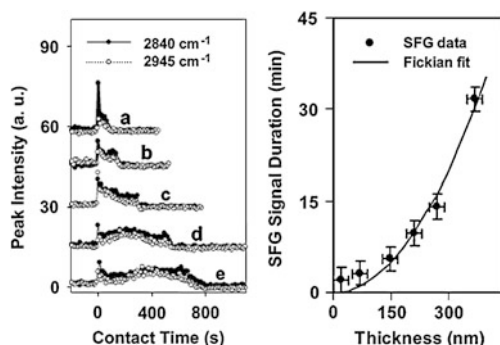


**Fig. 2.13** (Left) Time-dependent SFG peak intensities (SSP) at 2840 and 2945  $\text{cm}^{-1}$  that follow the diffusion of N-(2-aminoethyl)-3-aminopropyltrimethoxysilane through d-PMMA films of thicknesses (a) 20, (b) 70, (c) 150, (d) 210 and (e) 269 nm. (Right) SFG signal duration vs. film thickness showing the fit of a Fickian diffusion model. Reprinted from Ref. [77] with kind permission of © The American Chemical Society (2004)

in moisture-cured silicone sealants and adhesives. Unfortunately, amine groups are known to inhibit the Pt-catalyzed hydrosilylation crosslinking reactions commonly used for heat-cured silicone elastomers such as Sylgard® 184. Such addition cured materials are preferred in fast assembly processes that require a fast controllable cure with no volatile products, such as found in potting and lid sealing of automotive electronic modules or in the attachment of dies and heat sinks on microprocessors. A more commonly used system for promoting adhesion in Pt-cured elastomers utilizes a combination of 3-glycidoxypentyltrimethoxysilane ( $\gamma$ -GPS) and a methylvinylsiloxane diol oligomer (MVS) [78, 79]. Just 1–3 wt.% of this combination of additives mixed into a silicone elastomer can enable good primerless adhesion to a variety of metals and some polar plastics found in electronics applications such as polyesters or FR-4 fiberglass-epoxy composites used in circuit boards when cured at a suitable temperature. Recent studies with this system serve to further illustrate how SFG can be used to shed light and advance fundamental understanding of important and complex problems in adhesion promotion.

The general design concept behind such adhesion-promoting systems combines the reactivity of the  $\gamma$ -GPS to various substrates with the ability of the MVS to couple to the curing silicone elastomer through hydrosilylation of the pendant vinyl groups, and to the  $\gamma$ -GPS through condensation of the silanol ends with the alkoxysilane headgroup of  $\gamma$ -GPS by the following scheme:  $-\text{SiOH}$  (MVS) +  $-\text{SiOR}$  ( $\gamma$ -GPS)  $\rightarrow$   $-\text{Si-O-Si-}$  + ROH. However, because of the number of potential competing reactions among the additives, substrate and matrix, and the limited sensitivity of conventional surface analytical techniques to study small concentrations of silane additives against a strong bulk siloxane background, further detailed mechanistic understanding of bonding is limited. For instance, one can question whether epoxy ring opening is necessary for adhesion, or whether it merely serves as a driver for interfacial segregation of the  $\gamma$ -GPS through limiting the miscibility of GPS in the PDMS matrix. A number of studies of silane coupling agents on porous surfaces suggest that an interpenetrating resinous silsesquioxane network



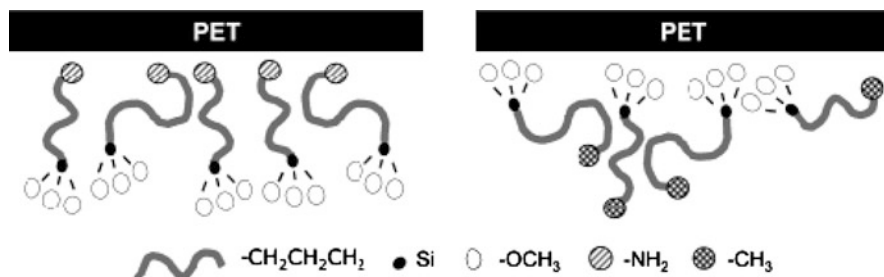


**Fig. 2.14** Schematic representations of the conformations of the silane molecules at the PET/ATMS (*left*) and PET/BTMS (*right*) interfaces. Reprinted from Ref. [83] with kind permission of © The American Chemical Society (2004)

can form at the adhesive/substrate interface, or more appropriately ‘interphase’, as the result of diffusion into the substrate surface followed by auto-condensation of the silane headgroups [80, 81]. Of course, this can only occur in cases where the substrate is sufficiently porous or penetrable by the silanes. For amorphous glassy polymers such as PS or PMMA, SFG studies by Loch et al. indicate that significant diffusion of  $\gamma$ -GPS can occur, to the point where the thin films are, respectively, swollen or altogether dissolved, within an hour of ambient exposure [82].

#### 2.3.3.2.4 H-Bonding Between Silane Adhesion Promoters and Polar Substrates

Many commercially important engineering plastics such as polyesters and polyamides are semi-crystalline and therefore less penetrable by adhesion promoters, presenting more stringent challenges to primerless adhesion. In studies using polyethylene terephthalate (PET) thin films as a model semi-crystalline substrate, Loch et al. observed the formation of stable interface signals between PET and aminopropyltrimethoxysilane (ATMS) and butyltrimethoxysilane (BTMS) due to the absence of silane diffusion [83]. A substantial shift in the  $-\text{C}=\text{O}$  peak stretch of PET at the PET/ATMS interface ( $1715\text{ cm}^{-1}$ ) relative to its original position of  $1725\text{ cm}^{-1}$  at the PET/air, PET/ $\gamma$ -GPS and PET/BTMS interfaces gave direct evidence of hydrogen bonding between PET and the  $-\text{NH}_2$  tail of ATMS. Further, by preparing PET films on a fused silica substrate with a nonresonant  $\text{TiO}_2$  interlayer, they compared the interface signals from the PET/ATMS surface against the PET/BTMS and deduced that ATMS oriented strongly to maximize favorable contacts between the  $-\text{NH}_2$  tail and the PET surface, in contrast to BTMS which takes on an opposite net orientation at the PET surface (Fig. 2.14).

#### 2.3.3.2.5 Adhesion Promoter Segregation

The aforementioned adhesion-promoting mixtures of  $\gamma$ -GPS and MVS were studied in various ratios against PET with perdeuterated glycol units (d-PET) [84]. It was found that the methoxy peak at  $2835\text{ cm}^{-1}$  and a peak at  $2950\text{ cm}^{-1}$  became stronger as the  $\gamma$ -GPS was effectively diluted by blending with MVS

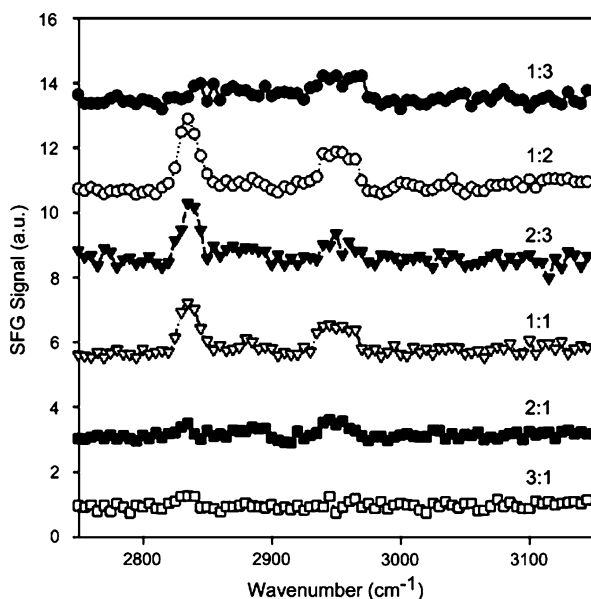


**Fig. 2.15** Stable SFG spectra (SSP) collected from the interfaces between d-PET and mixtures comprising different  $\gamma$ -GPS/MVS ratios. Reprinted from Ref. [84] with kind permission of © The American Chemical Society (2006)

(Fig. 2.15). If either component were diluted beyond 1:2 or 2:1 ratios, the SFG signal strength became notably weaker at these positions, suggesting that MVS plays a role in enhancing the net orientational order of  $\gamma$ -GPS at the interface. Comparisons at 1:1 ratios of  $\gamma$ -GPS to dimethylsiloxanol oligomer of similar chain length and to octamethyltrisiloxane show spectral features and intensity to 1:1  $\gamma$ -GPS:MVS, indicating this silane order-enhancing effect can be generalized to other siloxane oligomers. However, when MVS was studied in mixtures with two non-adhesion-promoting silanes, *n*-octadecyltrimethoxysilane and (tridecafluoro-1,1,2,2-tetrahydrooctyl)-trimethoxysilane, no enhancement in the order of the silane was observed [85]. Interestingly, a  $\gamma$ -GPS:MVS ratio close to 1:1 (w/w) is often used in practice because it generally gives the best adhesion. Therefore, these results motivate further studies to understand whether this observation is simply coincidental or whether interfacial silane ordering is a pre-requisite condition for adhesion.

#### 2.3.3.2.6 Cure Temperature Effects on Primerless Silicone Adhesives

Having established feasibility of interrogating adhesion promoter-polymer interactions through SFG, we proceed to the more complex problem of seeking correlations between practical adhesion and the interfacial concentration, ordering and reactivity of adhesion promoters diluted within a primerless silicone adhesive matrix. Loch et al. showed that even at just 1–2 wt.% of  $\gamma$ -GPS blended into uncured Sylgard® 184, SFG could detect a peak at  $2840\text{ cm}^{-1}$  characteristic of the methoxysilane

headgroup after curing against PET [86, 87]. Hence, as in the case of oligomeric siloxanes, it appears that the presence of a siloxane matrix helps induce enrichment and/or ordering of the silane at the substrate interface.

It should be noted that the development of adhesion in Pt-cured silicone elastomers to most substrates depends strongly upon temperature. Generally, a higher temperature is needed to develop adhesion than to merely cure the material for a given time. This effect can be studied easily by using a linear thermal gradient hot-plate such as that developed by Meredith et al. for high throughput and combinatorial studies of polymers [88]. Ahn et al. developed a methodology to study the effects of cure temperature on the adhesion of Pt-cured adhesives by curing a peel test specimen on the thermal gradient hot plate [44]. Because any position on the sample can be precisely mapped to a cure temperature, this approach allows one to probe correlations between thermal history (which is directly given by interface position), peeling behavior and interface composition through surface analysis in a continuous fashion. A peel test can be performed by initiating an interfacial crack at the originally cool end of the sample, which is then allowed to propagate along the temperature gradient, to expose an interface of linearly increasing cure temperature history. As the critical temperature ( $T_{CF}$ ) needed for adhesion is reached, the crack arrests at a position where the failure mode switches from interfacial failure to cohesive failure within the adhesive. One can then study either side of the exposed interface by a variety of conventional surface analytical techniques to determine how the interface composition and/or structure evolves as  $T_{CF}$  is reached asymptotically. Conveniently, this technique can also yield the temperature needed to cure ( $T_{Cure}$ ) the sample by simple measurement of the position where the adhesive transforms from a liquid to a solid.

For instance, Sylgard® 184 elastomer containing 1.5 wt.%  $\gamma$ -GPS cures in 1 h at  $T_{Cure} = 50^\circ\text{C}$  but has to be heated to nearly  $150^\circ\text{C}$  to develop adhesion to PET in the same time. The addition of an additional 1.5 wt.% of MVS can reduce the thermal requirement for adhesion significantly ( $T_{CF} = 86^\circ\text{C}$ ), while also raising the  $T_{Cure}$  to  $81^\circ\text{C}$ .<sup>3</sup> Hence, one can infer that adhesion is an activated process that differs from crosslinking, but the molecular origins of this activation energy have not been elucidated. To this end, the thermal gradient testing protocol has been applied in conjunction with SFG to give insights to the buried interface composition and structure at temperatures even above the transition to cohesive failure where conventional techniques are insensitive. Vasquez et al. showed that when samples are cured at temperatures above  $T_{CF}$  on d-PET there is actually a decrease in the methoxy stretch ( $2835\text{ cm}^{-1}$ ) from the  $\gamma$ -GPS headgroups, rather than an enhancement as observed for the aforementioned cases [87]. This result is consistent with a mechanism in which the adhesion to PET depends on reactivity of the alkoxy silane groups near  $T_{CF}$ . However, further studies are needed to establish whether these two events are directly correlated, and whether the origin of the signal loss is truly due to reaction of the methoxy groups, rather than diffusion (interface broadening) or

---

<sup>3</sup>The increase in cure temperature arises from mild Pt catalyst inhibition due to complexation between the Pt catalyst complex and the electron-rich adjacent vinyl groups of MVS.

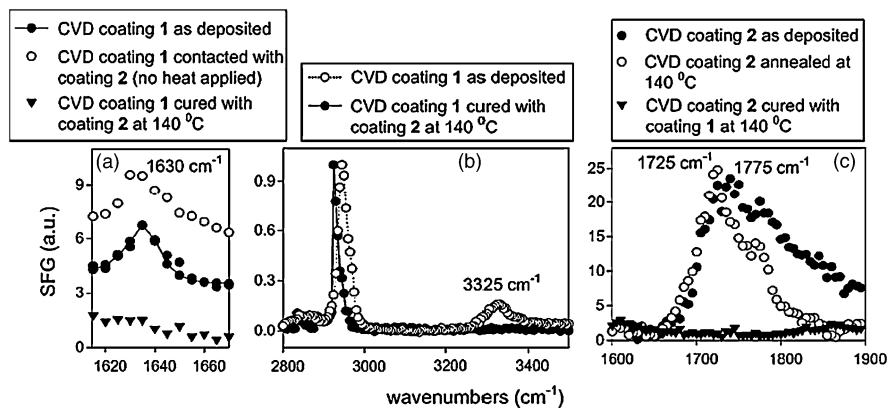


**Fig. 2.16** SFG spectra (SSP) of CVD-deposited poly(*p*-xylylenes) before and after bonding. Coating 1 is a primary amine PPX and Coating 2 is an aldehyde-functional PPX. (a) The NH<sub>2</sub> bending peak at 1635 cm<sup>-1</sup> before bonding, which disappears after bonding with coating 2. (b) The characteristic N-H stretching peak at 3325 cm<sup>-1</sup> before bonding, which disappears after bonding. (c) C=O stretching before bonding, and its disappearance after bonding. Reprinted from Ref. [89] with kind permission of ©The American Chemical Society (2008)

randomization near the interface. In particular, it would be particularly enlightening to develop sufficient signal strength to resolve the relatively weak epoxy ring C-H vibrations which so far have been gone undetected at these low concentrations of  $\gamma$ -GPS.

### 2.3.3.3 Adhesion of CVD-deposited films

Chen et al. studied the adhesion of cured Sylgard® 184 substrates that had been surface modified by CVD deposition of poly(*p*-xylylenes) (PPX) for microfluidic devices. By CVD-treating one substrate with amine-functional PPX and the second substrate with aldehyde-functional PPX then co-joining them at 140 °C, they observed strong adhesion resulting in cohesive failure of the silicone substrates [89]. As shown in Fig. 2.16, SFG was used to show the disappearance of amine (1635 cm<sup>-1</sup> and 3325 cm<sup>-1</sup>) and aldehyde (1725 cm<sup>-1</sup>) bands upon heating, providing evidence consistent with reactive coupling via imine bond formation at the interface between the opposing substrates. Spectral information regarding the interface between the PPX and silicone substrates was not reported.

### 2.3.4 Sensors

Sensors for chemical detection are another area where surface properties have strong impact on performance. The high gas permeability of siloxanes makes them quite useful matrices for sensors for gases and vapors. Selectivity and sensitivity to various analytes require incorporation of specific functional groups, whose structure

and proximity to the surface can presumably affect response strength and dynamics. Hartmann-Thompson et al. prepared a variety of coatings comprising hydrogen-bond acidic functional polyhedral oligosilsesquioxane (POSS) resins dispersed in siloxane or polycarbosilane matrices for chemical detecting surface acoustic wave sensors [90]. SFG studies of the free surfaces of these coatings spin coated onto quartz substrates indicated different levels of ordering of POSS at the free surface depending on loading in the matrix and upon the specific structure of the organofunctional groups decorating the vertices of the POSS cage. In the case where one of the vertices comprised an aliphatic hexafluoroalcohol group, a hydrogen-bonded OH band was observed at  $3470\text{ cm}^{-1}$  in SSP mode.

## 2.4 Conclusions and Future Directions

This chapter provides an overview of SFG vibrational spectroscopy and its use to study a variety of phenomena involving silicone surfaces and interfaces. We highlighted several examples of applications where SFG was used to provide unique insights to important problems related to the surface and interfacial behavior of silicones. However, SFG is still in its infancy as an analytical technique and perhaps somewhat under-utilized relative to other surface analysis techniques (see Chap. 12). This is in part due to limited awareness in the general materials research community of its capabilities coupled with the relatively limited number of available instruments and potential complexity of interpretation. As a nonlinear optical method, there are physical limits to the types of material, geometries and testing conditions that can be accommodated by SFG. It remains a highly specialized technique that is unlikely to surpass workhorse materials characterization techniques such as ATR-IR or contact angle goniometry in volume. However, from the standpoints of materials, instrumentation and analysis, we believe there remain many opportunities to increase utilization of SFG with silicone-based materials because of its unique surface sensitivity. Below are a number of topics where, to our knowledge, SFG has not yet been utilized but perhaps could be leveraged in the future to generate better understanding of phenomena relevant to silicones and siloxanes.

### 2.4.1 Materials

- (i) *Dispersed interfaces, filled systems* Many commercial silicone products contain fillers, pigments and other additives that introduce dispersed interfaces within the bulk of the silicone. In cases such as thermally or electrically conductive silicones, the structure of these dispersed interfaces can be critical to bulk performance. Even with adhesives and sealants, a reinforcing silica filler can act to absorb significant quantities of adhesion promoters designed to go to the substrate interface. In general, filled systems create difficulties for SFG analysis because the fillers tend to reduce transmission of IR and visible beams, and because they typically present non-uniform interfaces where inversion

symmetry is broken, generating an SFG signal which may or may not average to zero. For example, work with polymer-metal interfaces has been restricted to planar continuous interfaces [91]. However, there may be opportunities to test limits of SFG with dispersed interfaces in well characterized nanoparticle filled silicone elastomers where transparency is not sacrificed and where the particles have sufficient shape uniformity to behave isotropically in the bulk. Another example where SFG analysis could yield useful insights include correlations between filler surface chemistry, structure and alignment of anisotropic fillers with performance of thermally or electrically conductive silicones. Other areas of interest include characterization of particulate siloxanes and hybrid silicone-silicate materials. Intrinsically anisotropic materials such as Janus particles or rough surfaces in general are difficult to characterize by conventional means. For example, while the anisotropy of a densely packed array of Janus particles should generate differences in the signal from each hemisphere, structural inferences such as bond angle distributions would be obscured by the spherical surfaces. These considerations suggest SFG microscopy in conjunction with fast acquisition protocols might be useful in studying heterogeneous surfaces with micron-size surface topology.

- (ii) *Silicone surfactants* As discussed elsewhere in this volume (see Chap. 9), silicone surfactants are a powerful class of commercially important surfactants that can offer a rich variety of phase behavior. To our knowledge there has not been a systematic application of SFG to study and test correlations between surfactancy and molecular organization of functional groups in various architectures of silicone surfactants at air/water, oil/air and oil/water interfaces. We believe SFG may offer complementary insights to the current understanding and accelerate the ‘smart’ design of new silicone surfactants.
- (iii) *Crystalline and semi-crystalline siloxanes* The literature is predominantly focused on PDMS which is amorphous at ambient temperature and above. However, pure PDMS will crystallize around  $-50^{\circ}\text{C}$ , and many other siloxanes such as polydiethylsiloxane and polydiphenyl siloxane exhibit higher melting transitions. While bulk crystallization can be conveniently studied by x-ray techniques, the effects of surfaces and interfaces on controlling crystallinity of siloxanes is much less understood than in, say, polyolefins. We speculate that SFG may shed light on the effects of surfaces and interfaces on localized chain orientation in semi-crystalline siloxanes and liquid crystalline oligosiloxanes [92, 93].
- (iv) *Biological systems* We have not discussed the literature on silicone-biological interfaces in this chapter, as the applications of SFG have been limited to only a few studies involving silicones and silicone-modified organic copolymers such as polyurethane-PDMS block copolymers [56, 57]. Because of its inertness and stability in water, PDMS-based elastomers are widely used as substrates in biomedical devices and research in cellular biology. The development of microfluidic devices has spurred a number of studies of cell proliferation on PDMS elastomers modified by a variety of techniques to render the surface more hydrophilic and ‘cell-friendly’ [53, 94]. To our knowledge these studies

have not applied SFG to probe the molecular origins of the effects of surface modification on cell-polymer interactions.

### 2.4.2 Instrumentation and Techniques

- (i) *Turnkey SFG spectrometers* There have been considerable advances in SFG instrumentation over the last twenty years. The most critical element in the instrumentation is generation of a tunable high intensity infrared laser. Twenty years ago, the optical parametric amplifiers (OPA) were home built and there were very few laboratories equipped to do these measurements. In the last ten years many companies offered fully automated OPA and there are several companies who offer turnkey SFG systems [95]. In addition, we now have femtosecond systems based on Ti-sapphire lasers that can generate IR pulses ranging from 25 to 150 femtoseconds. With these advances the use of this technique is growing rapidly.
- (ii) *Dynamics and kinetics* With the introduction of the femtosecond laser systems in conjunction with CCD camera to detect SFG pulses it has become possible to acquire SFG spectra within msec [96]. This capability has opened the possibility to follow kinetics of diffusion and changes in the structure during frictional sliding. In addition, the pump-probe with femtosecond pulses offers possibilities of studying dynamics of PDMS chains at interfaces.
- (iii) *Extreme conditions* Most of the experiments with silicones to date have been conducted under ambient laboratory conditions. However, the transient behavior of many of the materials is strongly dependent on temperature and humidity. SFG instruments equipped with more sophisticated environmental controls to allow in situ studies of interface evolution with environmental conditioning should provide important insights on degradation mechanisms and suggest means to improve materials reliability.
- (iv) *Extension with high throughput or combinatorial methods* The thermal gradient experiments discussed above [44, 97] offer a glimpse at the possibility of combining a simple high throughput adhesion test method with SFG spectroscopy. Heightened interest and development of high throughput and combinatorial analytical methods over the past decade has yielded useful advances in automated sample processing and analysis that could be integrated with some aspects of SFG spectroscopy to make experimentation more efficient and analysis more informative.
- (v) *SFG mapping or imaging/microscopy* Industrial applications of polymers often involve blending of at least two polymers, block copolymers, small molecules, or composites. These systems are often phase separated and heterogeneous. The combination of SFG with microscopy could be valuable in studying such systems. Some initial progress has been reported in the literature on combining SFG with microscopy [98] and offers future possibility of combining this approach to study problems related with adhesion, friction, and wetting.

**Acknowledgements** The authors would like to acknowledge helpful discussions with Professor Zhan Chen (DA) and support from Dow Corning Corporation (DA) and the National Science Foundation (AD, DA).

## References

1. Noll W (1968) Chemistry and technology of silicones. Academic Press, New York
2. Kim J, Chaudhury MK, Owen MJ (1999) Hydrophobicity loss and recovery of silicone HV insulation. *IEEE Trans Dielectr Electr Insul* 6:695
3. Warrick EL (1990) Forty years of firsts: recollections of a Dow Corning pioneer. McGraw-Hill, New York
4. Shen YR (1996) A few selected applications of surface nonlinear optical spectroscopy. *Proc Natl Acad Sci USA* 93(22):12104–12111
5. Chen Z, Shen YR, Somorjai GA (2002) Studies of polymer surfaces by sum frequency generation vibrational spectroscopy. *Annu Rev Phys Chem* 53(1):437–465
6. Miranda PB, Shen YR (1999) Liquid interfaces: a study by sum-frequency vibrational spectroscopy. *J Phys Chem B* 103(17):3292–3307
7. Lambert AG, Davies PB, Neivandt DJ (2005) Implementing the theory of sum frequency generation vibrational spectroscopy: a tutorial review. *Appl Spectrosc Rev* 40(2):103–145
8. Morita A, Ishiyama T (2008) Recent progress in theoretical analysis of vibrational sum frequency generation spectroscopy. *Phys Chem Chem Phys* 10(38):5801–5816
9. Gracias DH, Chen Z, Shen YR, Somorjai GA (1999) Molecular characterization of polymer and polymer blend surfaces. Combined sum frequency generation surface vibrational spectroscopy and scanning force microscopy studies. *Acc Chem Res* 32:930–940
10. Chen Z (2010) Investigating buried polymer interfaces using sum frequency generation vibrational spectroscopy. *Prog Polym Sci* 35(11):1376–1402
11. Hirose C, Akamatsu N, Domen K (1992) Formulas for the analysis of the surface SFG spectrum and transformation coefficients of Cartesian SFG tensor components. *Appl Spectrosc* 46(6):1051–1072
12. Hirose C, Akamatsu N, Domen K (1992) Formulas for the analysis of surface sum frequency generation spectrum by CH stretching modes of methyl and methylene groups. *J Chem Phys* 96(2):997–1004
13. Shen YR (ed) (1984) The principles of nonlinear optics. Wiley, New York
14. Zhuang X, Miranda PB, Kim D, Shen YR (1999) Mapping molecular orientation and conformation at interfaces by surface nonlinear optics. *Phys Rev B* 59(19):12632
15. The theory section was reproduced with permission from Rangwalla H, Dhinojwala A (2004) *J Adhesion* 80:37–59
16. Watanabe N, Yamamoto H, Wada A, Domen K, Hirose C, Ohtake T, Mino N (1994) Vibrational sum-frequency generation (VSFG) spectra of *n*-alkyltrichlorosilanes chemisorbed on quartz plate. *Spectrochim Acta, Part A, Mol Biomol Spectrosc* 50(8–9):1529–1537
17. Simpson GJ, Rowlen KL (1999) An SHG magic angle: dependence of second harmonic generation orientation measurements on the width of the orientation distribution. *J Am Chem Soc* 121(11):2635–2636
18. Harp GP, Gautam KS, Dhinojwala A (2002) Probing polymer/polymer interfaces. *J Am Chem Soc* 124(27):7908–7909
19. Löbau J, Wolfrum K (1997) Sum-frequency spectroscopy in total internal reflection geometry: signal enhancement and access to molecular properties. *J Opt Soc Am B* 14(10):2505–2512
20. Wilson PT, Briggman KA, Wallace WE, Stephenson JC, Richter LJ (2002) Selective study of polymer/dielectric interfaces with vibrationally resonant sum frequency generation via thin-film interference. *Appl Phys Lett* 80(17):3084–3086



21. Wang J, Chen C, Buck SM, Chen Z (2001) Molecular chemical structure on poly(methyl methacrylate) (PMMA) surface studied by sum frequency generation (SFG) vibrational spectroscopy. *J Phys Chem B* 105(48):12118–12125
22. Gautam KS, Dhinojwala A (2001) Molecular structure of hydrophobic alkyl side chains at comb polymer-air interface. *Macromolecules* 34(5):1137–1139
23. Gautam KS, Dhinojwala A (2002) Melting at alkyl side chain comb polymer interfaces. *Phys Rev Lett* 88(14):145501
24. Harp GP, Rangwalla H, Yeganeh MS, Dhinojwala A (2003) Infrared-visible sum frequency generation spectroscopic study of molecular orientation at polystyrene/comb-polymer interfaces. *J Am Chem Soc* 125(37):11283–11290
25. Harp GP, Rangwalla H, Li G, Yeganeh MS, Dhinojwala A (2006) Coupling of interfacial motion at polystyrene-alkane interfaces. *Macromolecules* 39(22):7464–7466
26. Nanjundiah K, Dhinojwala A (2005) Confinement-induced ordering of alkanes between an elastomer and a solid surface. *Phys Rev Lett* 95(15):154301
27. Nanjundiah K, Hsu PY, Dhinojwala A (2009) Understanding rubber friction in the presence of water using sum-frequency generation spectroscopy. *J Chem Phys* 130(2):024702
28. Li G, Dhinojwala A, Yeganeh MS (2011) Interference effect from buried interfaces investigated by angular-dependent infrared—visible sum frequency generation technique. *J Phys Chem C* 115(15):7554–7561
29. Schwab AD, Dhinojwala A (2003) Relaxation of a rubbed polystyrene surface. *Phys Rev E* 67(2):021802
30. Oh-e M, Hong S-C, Shen YR (2002) Orientations of phenyl sidegroups and liquid crystal molecules on a rubbed polystyrene surface. *Appl Phys Lett* 80(5):784–786
31. Prasad S, Hanne L, Dhinojwala A (2005) Thermodynamic study of a novel surface ordered phase above the bulk melting temperature in alkyl side chain acrylate polymers. *Macromolecules* 38(7):2541–2543
32. Zhang D, Dougal SM, Yeganeh MS (2000) Effects of UV irradiation and plasma treatment on a polystyrene surface studied by IR—visible sum frequency generation spectroscopy. *Langmuir* 16(10):4528–4532
33. Rangwalla H, Schwab AD, Yudumakan B, Yablon DG, Yeganeh MS, Dhinojwala A (2004) Molecular structure of an alkyl-side-chain polymer-water interface: origins of contact angle hysteresis. *Langmuir* 20:8625–8633
34. Lachat V, Varshney V, Dhinojwala A, Yeganeh MS (2009) Molecular origin of solvent resistance of polyacrylonitrile. *Macromolecules* 42(18):7103–7107
35. Li G, Dhinojwala A, Yeganeh MS (2009) Interfacial structure and melting temperature of alcohol and alkane molecules in contact with polystyrene films. *J Phys Chem B* 113(9):2739–2747
36. Wilson PT, Richter LJ, Wallace WE, Briggman KA, Stephenson JC (2002) Correlation of molecular orientation with adhesion at polystyrene/solid interfaces. *Chem Phys Lett* 363(1–2):161–168
37. Kurian A, Prasad S, Dhinojwala A (2010) Unusual surface aging of poly(dimethylsiloxane) elastomers. *Macromolecules* 43(5):2438–2443
38. Clancy TC, Jang JH, Dhinojwala A, Mattice WL (2001) Orientation of phenyl rings and methylene bisectors at the free surface of atactic polystyrene. *J Phys Chem B* 105(46):11493–11497
39. Tsige M, Soddemann T, Rempe SB, Grest GS, Kress JD, Robbins MO, Sides SW, Stevens MJ, Webb E (2003) Interactions and structure of poly(dimethylsiloxane) at silicon dioxide surfaces: electronic structure and molecular dynamics studies. *J Chem Phys* 118(11):5132–5142
40. Yurdumakan B, Harp GP, Tsige M, Dhinojwala A (2005) Template-induced enhanced ordering under confinement. *Langmuir* 21(23):10316–10319
41. Brook MA (2000) Silicon in organic, organometallic and polymer chemistry. Wiley, New York
42. Skeist I (ed) (1990) Handbook of Adhesive, 3rd edn. Van Nostrand Reinhold, New York

43. Ahn D, Lipp ED, McMillan CS (2003) Improved self-priming silicone adhesives through selective interfacial enrichment. In: Proceedings 26th annual meeting of the adhesion society. Adhesion Society, Blacksburg, pp 430–432
44. Ahn D, Shephard NE, Olney PA, McMillan CS (2007) Thermal gradient enabled XPS analysis of PDMS elastomer adhesion to polycarbonate. *Macromolecules* 40(11):3904–3906
45. Smith AL (ed) (1991) *The analytical chemistry of silicones*. Wiley-Interscience, New York
46. Zhou X, Hu S, Shephard NE, Ahn D (2003) Diffusion-controlled titanate-catalyzed condensation of alkoxy silanes in nonpolar solvents. In: *Synthesis and properties of silicones and silicone-modified materials*. ACS symposium series, vol 838, pp 375–387
47. Comyn J, de Buyl F, Comyn TP (2003) Diffusion of adhesion promoting and crosslinking additives in an uncured silicone sealant. *Int J Adhes Adhes* 23(6):495–497
48. Comyn J, de Buyl F, Shephard NE, Subramaniam C (2002) Kinetics of cure crosslink density and adhesion of water-reactive alkoxy silicone sealants. *Int J Adhes Adhes* 22(5):385–393
49. Gordon GVL, Loren D (2008) A generalized cure model for one-part RTV sealants and adhesives. In: *Proceedings of the annual meeting of the adhesion society*, pp 298–300
50. Ismail AE, Grest GS, Heine DR, Stevens MJ, Tsige M (2009) Interfacial structure and dynamics of siloxane systems: PDMS-vapor and PDMS-water. *Macromolecules* 42(8):3186–3194
51. Chen CY, Wang J, Chen Z (2004) Surface restructuring behavior of various types of poly(dimethylsiloxane) in water detected by SFG. *Langmuir* 20:10186–10193
52. Lee SH, Ruckenstein E (1987) Surface restructuring of polymers. *J Colloid Interface Sci* 120(2):529–536
53. Park JY, Ahn D, Choi YY, Hwang CM, Takayama S, Lee SH, Lee S-H (2011) Surface chemistry modification of PDMS elastomers with boiling water improves cellular adhesion. Manuscript submitted for publication
54. Kurian A, Prasad S, Dhinojwala A (2010) Unusual surface aging of poly(dimethylsiloxane) elastomers. *Macromolecules* 43:2438–2443
55. Yurdumakan B, Nanjundiah K, Dhinojwala A (2006) Origin of higher friction for elastomers sliding on glassy polymers. *J Phys Chem C* 111(2):960–965
56. Ye S, Majumdar P, Chisholm B, Stafslie S, Chen Z (2010) Antifouling and antimicrobial mechanism of tethered quaternary ammonium salts in a cross-linked poly(dimethylsiloxane) matrix studied using sum frequency generation vibrational spectroscopy. *Langmuir* 26(21):16455–16462
57. Chen Z, Ward R, Tian Y, Eppler AS, Shen YR, Somorjai GA (1999) Surface composition of biopolymer blends biospan-SP/phenoxy and biospan-F/phenoxy observed with SFG, XPS, and contact angle goniometry. *J Phys Chem B* 103(15):2935–2942
58. Ye H, Gu Z, Gracias DH (2006) Kinetics of ultraviolet and plasma surface modification of poly(dimethylsiloxane) probed by sum frequency vibrational spectroscopy. *Langmuir* 22(4):1863–1868
59. Ouyang M, Yuan C, Muisener RJ, Boulares A, Koberstein JT (2000) Conversion of some siloxane polymers to silicon oxide by UV/ozone photochemical processes. *Chem Mater* 12(6):1591–1596
60. Schnyder B, Lippert T, Kötzt R, Wokaun A, Graubner V-M, Nuyken O UV-irradiation induced modification of PDMS films investigated by XPS and spectroscopic ellipsometry. *Surf Sci* 532–535, 1067–1071 (2003)
61. Graubner V-M, Jordan R, Nuyken O, Schnyder B, Lippert T, Kötzt R, Wokaun A (2004) Photochemical modification of cross-linked poly(dimethylsiloxane) by irradiation at 172 nm. *Macromolecules* 37(16):5936–5943
62. Efimenko K, Wallace WE, Genzer J (2002) Surface modification of Sylgard-184 poly(dimethyl siloxane) networks by ultraviolet and ultraviolet/ozone treatment. *J Colloid Interface Sci* 254(2):306–315
63. Harp GP, Dhinojwala A (2005) Direct probe of interfacial structure during mechanical contact between two polymer films using infrared visible sum frequency generation spectroscopy. *J Adhes* 81(3–4):371–379
64. Schallamach A (1963) A theory of dynamic rubber friction. *Wear* 6(5):375–382

65. Kurian A, Prasad S, Dhinojwala A (2010) Direct measurement of acid-base interaction energy at solid interfaces. *Langmuir* 26(23):17804–17807
66. Roberts AD, Tabor D (1971) The extrusion of liquids between highly elastic solids. *Proc R Soc London, Ser A* 325(1562):323–345
67. Israelachvili JN (1991) *Intermolecular & surface forces*, 2nd edn. Academic Press, San Diego
68. Andrews EH, Kinloch AJ (1973) *Proc R Soc London, Ser A* 332:385
69. Gent AN, Schultz J (1972) *J Adhes* 3:281
70. Ferry JD (ed) (1980) *Viscoelastic properties of polymers*, 3rd edn. Wiley, New York
71. Roan GA (2003) Advances in acrylic hybrid technology. *Adhes Sealants Industry* 2003:36–40
72. Schmidt RG, Gordon GV, Dreiss CA, Cosgrove T, Krukonijs VJ, Williams K, Wetmore PM (2010) A critical size ratio for viscosity reduction in poly(dimethylsiloxane)-polysilicate nanocomposites. *Macromolecules* 43(23):10143–10151
73. Gordon GV, Schmidt RG, Quintero M, Benton NJ, Cosgrove T, Krukonijs VJ, Williams K, Wetmore PM (2010) Impact of polymer molecular weight on the dynamics of poly(dimethylsiloxane)-polysilicate nanocomposites. *Macromolecules* 43(23):10132–10142
74. Gordon GV, Perz SV, Tabler RL, Stasser JL, Owen MJ, Tonge JS (1998) Silicone release coatings: a closer look at release mechanisms. [www.dowcorning.com/content/publishedlit/26-016.pdf](http://www.dowcorning.com/content/publishedlit/26-016.pdf). Dow Corning Corporation, Midland, MI
75. Plueddemann EP (ed) (1991) *Silane coupling agents*, 2nd edn. Plenum Press, New York
76. Chen C, Loch CL, Wang J, Chen Z (2003) Different molecular structures at polymer/silane interfaces detected by SFG. *J Phys Chem B* 107:10440–10445
77. Chen C, Wang J, Loch CL, Ahn D, Chen Z (2004) Demonstrating the feasibility of monitoring the molecular-level structures of moving polymer/silane interfaces during silane diffusion using SFG. *J Am Chem Soc* 126(4):1174–1179
78. Mine K, Nishio M, Sumimura S (1977) Heat curable organopolysiloxane compositions containing adhesion additives. US Patent 4,033,924, July 5
79. Schulz JR (1978) Self-adhering silicone compositions and preparations thereof. US 4,087,585, May 2
80. Gellman AJ, Naasz BM, Schmidt RG, Chaudhury MK, Gentle TM (1990) Secondary neutral mass spectrometry studies of germanium-silane coupling agent-polymer interphase. *J Adhes Sci Technol* 4(7):597–601
81. Gentle TE, Schmidt RG, Naasz BM, Gellman AJ, Gentle TM (1992) Organofunctional silanes as adhesion promoters: direct characterization of the polymer/silane interphase. In: Mittal KL (ed) *Silanes and other coupling agents*. VSP, Utrecht, pp 295–304
82. Loch CL, Ahn D, Vazquez AV, Chen Z (2007) Diffusion of one or more components of a silane adhesion-promoting mixture into poly(methyl methacrylate). *J Colloid Interface Sci* 308(1):170–175
83. Loch CL, Ahn D, Chen C, Wang J, Chen Z (2004) Sum frequency generation studies at poly(ethylene terephthalate)/silane interfaces: hydrogen bond formation and molecular conformation determination. *Langmuir* 20:5467–5473
84. Loch CL, Ahn D, Chen CY, Chen Z (2006) Sum frequency generation vibrational spectroscopic studies on a silane adhesion promoting mixture at a polymer interface. *J Phys Chem B* 110:914–918
85. Vázquez AV, Boughton AP, Shephard NE, Rhodes SM, Chen Z (2009) Molecular structures of the buried interfaces between silicone elastomer and silane adhesion promoters probed by sum frequency generation vibrational spectroscopy and molecular dynamics simulations. *ACS Appl Mater Interfaces* 2(1):96–103
86. Loch CL, Ahn D, Chen Z (2005) Polymer-silane interactions probed by sum frequency generation vibrational spectroscopy. *J Adhes* 81:319–345
87. Vázquez AV, Shephard NE, Steinecker CL, Ahn D, Spanninga S, Chen Z (2009) Understanding molecular structures of buried polymer interfaces using sum frequency generation vibrational spectroscopy and relating interfacial structures to polymer adhesion. *J Colloid Interface Sci* 331(2):408–416
88. Meredith JC, Karim A, Amis EJ (2000) High-throughput measurement of polymer blend phase behavior. *Macromolecules* 33(26):5760–5762

89. Chen H-Y, McClelland AA, Chen Z, Lahann J (2008) Solventless adhesive bonding using reactive polymer coatings. *Anal Chem* 80(11):4119–4124
90. Hartmann-Thompson C, Keeley DL, Dvornic PR, Keinath SE, McCrea KR (2007) Hydrogen-bond acidic polyhedral oligosilsesquioxane filled polymer coatings for surface acoustic wave sensors. *J Appl Polym Sci* 104(5):3171–3182
91. Lu X, Li D, Kristalyn CB, Han J, Shephard N, Rhodes S, Xue G, Chen Z (2009) Directly probing molecular ordering at the buried polymer/metal interface. *Macromolecules* 42(22):9052–9057
92. Tschierske C (1998) Non-conventional liquid crystals-the importance of micro-segregation for self-organisation. *J Mater Chem* 8(7):1485–1508
93. Yoon H, Agra-Kooijman DM, Ayub K, Lemieux RP, Kumar S (2011) Direct observation of diffuse cone behavior in de Vries smectic-A and -C phases of organosiloxane mesogens. *Phys Rev Lett* 106(8):087801
94. Park JY, Hwang CM, Lee S-H (2008) Effective methods to improve the biocompatibility of poly(dimethylsiloxane). *BioChip J* 2(1):39–43
95. Smith JP, Hinson-Smith V (2004) Product review: SFG coming of age. *Anal Chem* 76(15):287 A-290
96. Richter LJ, Petralli-Mallow TP, Stephenson JC (1998) Vibrationally resolved sum-frequency generation with broad-bandwidth infrared pulses. *Opt Lett* 23(20):1594–1596
97. Vazquez AV, Shephard NE, Steinecker CL, Ahn D, Spanninga S, Chen Z (2009) Understanding molecular structures of silanes at buried polymer interfaces using sum frequency generation vibrational spectroscopy and relating interfacial structures to polymer adhesion. *J Colloid Interface Sci* 331(2):408–416
98. Hernandez M, Chinwangso P, Cimatu K, Srisombat L-O, Lee TR, Baldelli S (2011) Chemical imaging and distribution analysis of mono-, bi-, and tridentate alkanethiol self-assembled monolayers on gold by sum frequency generation imaging microscopy. *J Phys Chem C* 115(11):4688–4695



<http://www.springer.com/978-94-007-3875-1>

Silicone Surface Science

Owen, M.J.; Dvornic, P.R. (Eds.)

2012, XVI, 388 p., Hardcover

ISBN: 978-94-007-3875-1